



# Fluvial discharge and sea-level changes controlling black shale deposition during the Paleocene–Eocene Thermal Maximum in the Dababiya Quarry section, Egypt

Peter Schulte<sup>a,\*</sup>, Christian Scheibner<sup>b</sup>, Robert P. Speijer<sup>c</sup>

<sup>a</sup> GeoZentrum Nordbayern, Universität Erlangen, D-91054 Erlangen, Germany

<sup>b</sup> Department of Geosciences, Bremen University, P.O. Box 330440, D-28334 Bremen, Germany

<sup>c</sup> Department of Earth and Environmental Sciences, K.U.Leuven, B-3001 Leuven, Belgium

## ARTICLE INFO

### Article history:

Received 22 April 2010

Received in revised form 1 December 2010

Accepted 5 April 2011

Available online 12 April 2011

Editor: J.D. Blum

### Keywords:

Eocene

Continental shelf

Sequence stratigraphy

Hyperthermal

Carbon cycle

Ocean acidification

## ABSTRACT

The formation of black shales along the Tethyan margins at the Paleocene–Eocene Thermal Maximum (“PETM”; ~55 Ma) may have been an important feedback mechanism to reduce the warming by excess carbon burial. However, the detailed evolution of sediment redox conditions during this event is still poorly constrained. We address this issue by a high-resolution mineralogical and geochemical investigation of the outer neritic Dababiya Quarry PETM section in Central Egypt, which serves as the Global boundary Stratotype Section and Point for the base of the Eocene. There, the base of the PETM beds corresponds to the onset of sediment lamination indicative of oxygen-deficiency at the seafloor. The absence of calcium carbonate and a major increase in phyllosilicate abundance and change in detritus-sensitive trace elements is indicative of severe carbonate dissolution in addition to enhanced fluvial input, erosion of coastal low lands, and deposition during low or slightly rising sea level. Subsequently, fully anoxic conditions were established for a short period during the peak phase of the PETM as recorded by the strong relative enrichment of redox-sensitive trace elements and organic carbon compared to background sediments. The decoupling of the Fe and Mo contents from the detrital fraction may even indicate that euxinic conditions existed with free hydrogen sulfide in the water column. Concurrent to the onset of anoxia, high carbonate and quartz contents as well as high elemental ratios of Si/Al suggest a major drop of siliciclastic sediment supply (sediment starvation), most likely caused by a rapid sea level rise. The final recovery phase of the PETM is associated with a progressive restoration of the pre-PETM siliciclastic sedimentation, temporary (seasonal) anoxic to dysoxic conditions, and high phosphorus enrichment, followed by carbonate-dominated sedimentation and the return to well-oxygenated conditions.

We conclude that after a period of strong fluvial discharge, several parameters inherent to the PETM (e.g., warming, water-column stratification, and enhanced fluvial discharge) may have contributed to the development of anoxia and increased the burial efficiency of organic carbon by reducing water column oxygenation. The temporal coincidence of sediment starvation and onset of black shale deposition during the PETM suggests that a rapid sea-level rise was an additional important triggering factor. Therefore, our results support not only current views that Tethyan continental shelf areas may have acted as large carbon sinks during the PETM, but also indicate that transgressions may have provided an important feedback mechanism for organic carbon drawdown during hyperthermal events.

© 2011 Elsevier B.V. All rights reserved.

## 1. Introduction

The sudden and massive input of isotopically light carbon into the ocean–atmosphere system during the earliest Eocene (~55 Ma) had dramatic environmental consequences for the marine and terrestrial realms (e.g., Kennett and Stott, 1991; Dickens et al., 1995). Global temperatures increased by about 5 to 8 °C (Bowen et al., 2006; Sluijs et al., 2007) and large parts of the deep oceans were “acidified” (Zachos et al.,

2005). The onset of this Paleocene–Eocene Thermal Maximum (“PETM”), which is marked by a prominent negative carbon isotope excursion (“CIE”, Dickens et al., 1995), occurred rapidly within a few thousand years (“ky”) although the mechanisms for the carbon release and its amount are still unclear (Bains et al., 1999; Higgins and Schrag, 2006; Pagani et al., 2006a; Bowen and Bowen, 2008). The subsequent progressive return to pre-PETM environmental conditions occurred in less than ~200 ky (Röhl et al., 2007) and was possibly enhanced by CO<sub>2</sub>-triggered increased weathering and bioproductivity feedback effects. Thus, the environmental consequences of this event are very similar to the proposed consequences of the current large-scale CO<sub>2</sub> release (e.g., global warming and ocean acidification; Trenberth et al., 2007). Consequently, the PETM

\* Corresponding author.

E-mail address: [schulte@geol.uni-erlangen.de](mailto:schulte@geol.uni-erlangen.de) (P. Schulte).

may serve as a deep-time analog to illustrate the effects of global warming and inform the public to the sensitivity of the ocean–atmosphere system, although it is important to note that modern CO<sub>2</sub> release rates are possibly higher than those during the PETM.

The timing of the PETM, the extent of ocean acidification, and the associated extinction of benthic microfossils have been revealed mainly from pelagic sections while continental shelf sections provide a more detailed record of (i) the rapid sea-level rise of about 20 m presumably resulting from global warming and thermal ocean water mass expansion (Speijer and Morsi, 2002; Sluijs et al., 2008), (ii) variations in the detrital input, reflecting enhanced continental weathering regimes due to higher temperatures and an accelerated hydrological cycle (Gibson et al., 2000; Schmitz et al., 2001), and (iii) accumulations of organic carbon-rich sediments, that may be related to productivity-feedback mechanisms (Speijer and Wagner, 2002; Crouch et al., 2003; John et al., 2008), ultimately bringing down elevated CO<sub>2</sub> concentrations in the ocean–atmosphere system. Specifically, the occurrence of unusual organic-rich sediments during the PETM in the Tethyan realm suggests that the continental shelves may have acted as important carbon sinks, counterbalancing the massive carbon input at the onset of the CIE (Speijer and Wagner, 2002; Gavrillov et al., 2003; John et al., 2008).

Situated on the southern Tethyan margin (Fig. 1), the Dababiya Quarry section in central Egypt (Figs. 2 and 3), is considered as one of the most complete PETM sections. Many detailed environmental studies are available, although research has concentrated on the faunal response to the PETM (e.g., Dupuis et al., 2003; Ernst et al., 2006; Aubry et al., 2007) and only one petrographic and geochemical study has been conducted (Soliman et al., 2006). Key characteristics of the Dababiya Quarry section are the relatively gradual onset of the CIE, the presence of a basal phyllosilicate-rich interval that is deprived in calcium carbonate and overlain by a meter-thick black shale sequence rich in organic matter and phosphorus (Fig. 4). This sedimentary sequence was deposited at fully marine conditions at outer-shelf settings. Thus, the Dababiya section may be ideally suited to provide an expanded record of environmental changes across the PETM and address the following two issues:

First, previous investigations have shown that prominent mineralogical changes occurred at the onset of the PETM suggesting either progressive erosion of proximal areas during a rapid sea-level rise (Dupuis et al., 2003; Ernst et al., 2006) or increased weathering recorded by a pulse-like kaolinite input during the PETM (Bolte and Adatte, 2001). We incorporate mineralogical analysis and detritus-

characterizing elements in addition to rare-earth elements to determine changes in sediment provenance, to discriminate between these scenarios, and to refine them.

Second, it was suggested that the lower part of the PETM sequence was deposited under euxinic conditions leading to the mass mortality of benthic life and black shale formation (e.g., Soliman et al., 2006; Aubry et al., 2007). Moreover, the PETM “can lay claim, if not to being the last oceanic anoxic event of the Phanerozoic, to at least sharing many features in common” (p. 19, Jenkyns, 2010). Upwelling of low-oxygen intermediate Tethyan water onto the southern Egyptian shelf has been considered as one scenario to promote sea-floor anoxia during the PETM (Speijer and Wagner, 2002; Soliman et al., 2006). However, this scenario has not yet been further evaluated. To detail the degree, stratigraphic position, and possible causes of anoxia, we make use of the detritus-characterizing elements as outlined above and also analyzed a suite of redox-sensitive trace elements to compare them with results from other black shale deposits in the geological record. Specifically, we investigate the possible role of sea-level fluctuations for initiating anoxia during the PETM. Although much debate has focused on the roles of production (e.g., Pedersen and Calvert, 1990) versus preservation (e.g., Demaison and Moore, 1980) of organic carbon under anoxic conditions, recent studies have suggested that such an “either/or” view is probably too simplistic (Arthur and Sageman, 1994; Canfield, 1994; Murphy et al., 2000). Consequently, changes in relative sea level and related variations in sediment grain size, sedimentation rate (condensation), and oceanographic circulation as well as changes in biogeochemical (re)cycling are now recognized as important contributing factors in the accumulation of organic-rich deposits (e.g., Tyson and Pearson, 1991; Murphy et al., 2000; Wignall and Newton, 2001; Werne et al., 2002; Arthur and Sageman, 2005; White and Arthur, 2006; Rabalais et al., 2009).

## 2. Material and methods

The El Dababiya Quarry Member that records the PETM sequence occurs throughout the Upper Nile Valley, in the Western (Kharga Oasis) and in the Eastern Desert (Duwi Section) (Fig. 2; Ouda, 2003). This study focuses on the Dababiya Quarry section, which is located near the

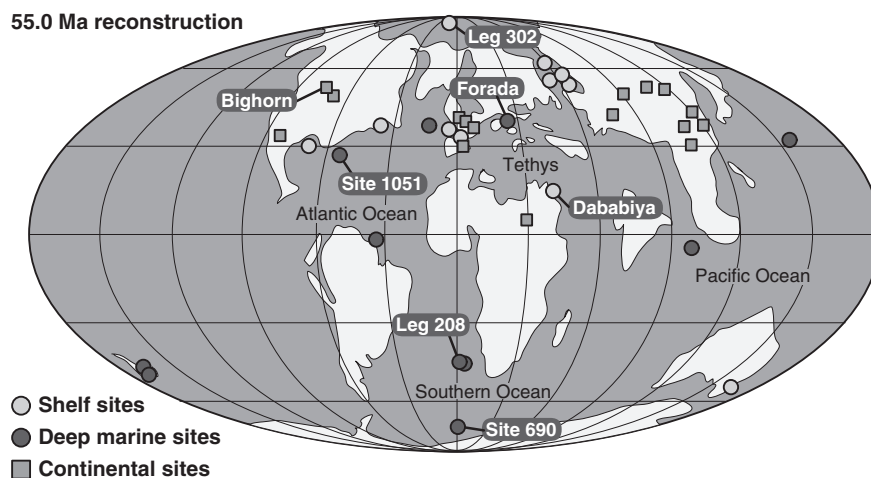
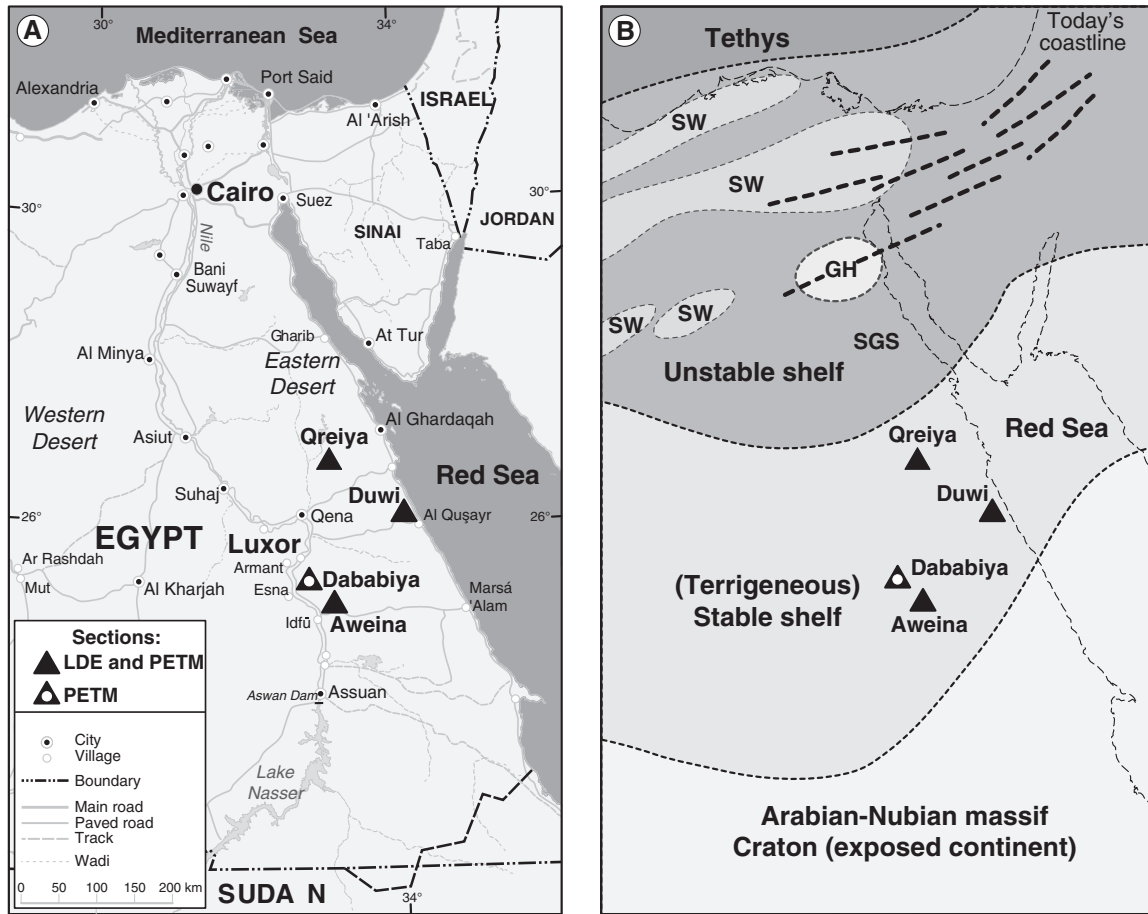


Fig. 1. Paleogeographic location of the Dababiya Quarry section and other important PETM sites. Reconstruction from <http://www.ods.de>.



**Fig. 2.** (A) Overview map of Egypt showing the sections that include the Paleocene–Eocene Thermal Maximum (PETM) as well as the Latest Danian Event (LDE). (B) Simplified map of the Early Eocene southern Tethys margin in Egypt showing the location of the emerged Galala High (GH), the Southern Galala Subbasin (SGS) and other submarine swells (SW) according to Höntzsch et al. (2011). The position of stable and unstable shelf was estimated by Meshref (1990) and was modified for the Early Palaeogene by Scheibner et al. (2001) and Speijer and Wagner (2002). The faults (thick dashed lines) in the northeastern area belong to the Syrian Arc fold belt.

ancient quarry east of the village of Dababiya in the Eastern Desert close to the Nile Valley (Fig. 3, Dupuis et al., 2003). The studied samples were collected from a few meters south of the protected GSSP section of the basal Eocene, also known as the DBH section (25°30'N, 32°31'52"E; Dupuis et al., 2003; Ernst et al., 2006). Since the beds show very little dip, the sequence is identical to the GSSP section (Fig. 3).

To obtain fresh rock, the samples were collected from the vertical quarry face of the Dababiya outcrop. Grain-size analysis on the insoluble residue of selected samples was conducted at the University of Erlangen. For mineralogical analysis, samples were ground with a McCrone Micromill to obtain a consistent grain size of <10 µm by using 3 g of sample material, 5 ml of Isopropanol and grinding times of 4 min. For clay mineralogy, the decalcified <2 µm fraction was saturated with MgCl<sub>2</sub>, sucked through a ceramic filter, and analyzed as air-dried, glycolated, and heated (450 °C for 1 h) specimens before X-ray analysis from 3 to 36° 2θ in steps of 0.02° at 2 seconds per step. The mineralogical composition of the powdered samples was determined at the University of Erlangen using a Siemens D5000 X-ray diffractometer. This instrument is fitted with a copper tube (Cukα = 1.54178 Å), operating at 40 kV and 35 mA, and a post-diffraction graphite monochromator. Samples were scanned from 5° to 65° 2θ in steps of 0.02° and 4 s scanning time.

The Rietveld analysis of the bulk rock XRD scans was conducted with the BGMN 5.0.12 software. The quality of the Rietveld refinement was very good and the observed weighted residual errors  $R_{wp}$  ranged from approximately 8.5 to 12.5% (Appendix A of the Supplementary data). Also, the weighted residual errors  $R_{wp}$  approach the statistically

expected values  $R_{exp}$ , indicating very good agreement between the observed and simulated XRD patterns. Also, the calculated quality parameter  $1-\rho$  ranged from excellent values as low as 1.3 to higher values of about 3.5% (Appendix A). The higher values of  $1-\rho$  are confined to calcite-poor and illite-smectite-rich samples of DQBed 1 and are probably related to compositional changes in the smectite mineralogy that were not considered in the present study. To address precision of the XRD analysis, multiple preparations and subsequent analysis of a single sample were conducted resulting in an interquartile range of the major mineral phases in the acceptable range of about 0.5 to 1 wt.%. The accuracy of the quantitative Rietveld refinement was tested by several representative samples spiked with 10 wt.% zincite (ZnS) as an internal standard. This standard could be recovered satisfactorily by all refinements, although a tendency towards higher values is obvious (~11.5 wt.% to ~14 wt.%). These overestimations are mostly related to the presence of additional X-ray amorphous components including organic material, as confirmed by the elevated TOC values shown in Fig. 4.

The bulk major elements (Na, Mg, Al, Si, P, S, K, Ca, Ti, and Fe) and a range of trace elements (Mn, V, Cr, Co, Ni, Cu, Zn, As, Rb, Sr, Zr, Nb, Mo, and Ba) were analyzed in 27 samples by means of X-ray fluorescence (XRF) at the Geosciences Department of the University of Bremen (Appendix B and C). Samples were finely ground and homogenized in an agate mortar and prepared for major and trace element determination. For major element analysis, glass discs were processed by melting about 0.3 g of ground bulk sediment with a Li tetra borate flux. For trace element analysis, discs were produced by pressing about 5 g of ground

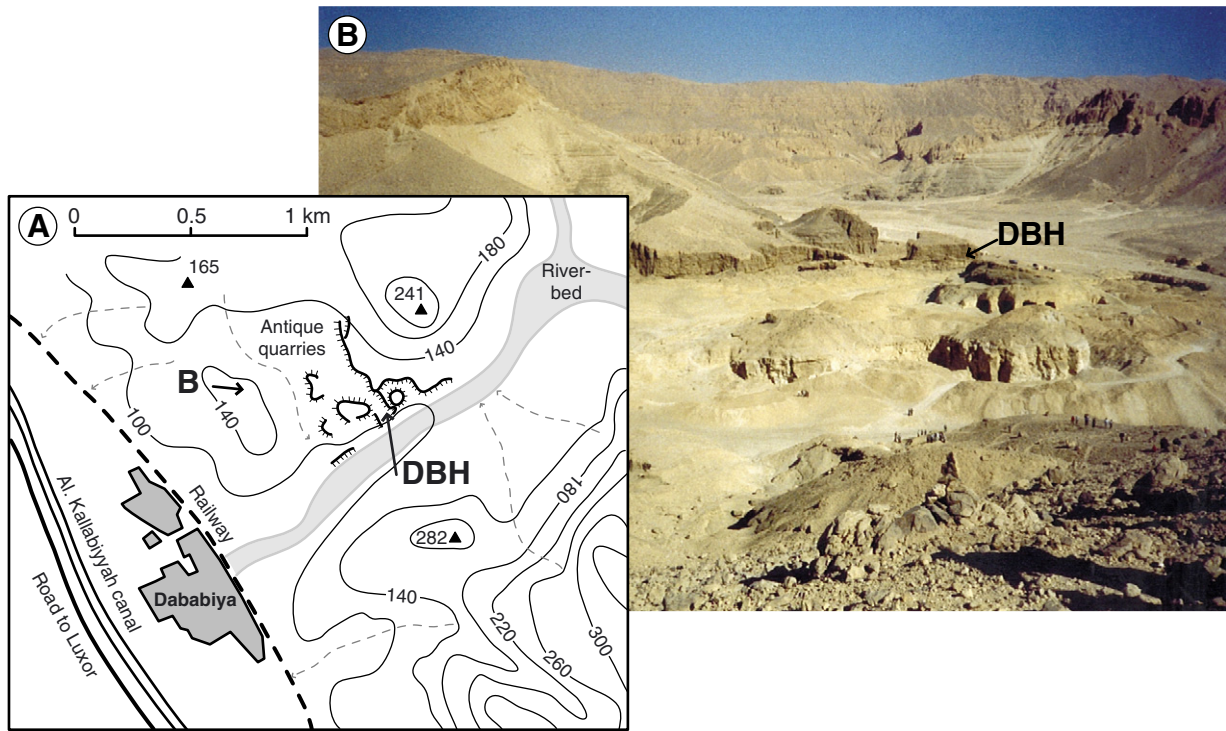


Fig. 3. Detail map (A) and image (B) of the Dababiya Quarry area with the position of the studied DBH section. Map modified from Aubry et al. (2007).

bulk sediment into a briquet, with boric acid backing. XRF analyses were performed with a Philips PW 2400 sequential wavelength dispersive X-ray spectrometer. Analytical accuracy was checked measuring five

international standards (GSS-1 to GSS-5) and precision was determined by replicate analyses of samples (0.8% for major and 4% for trace elements).

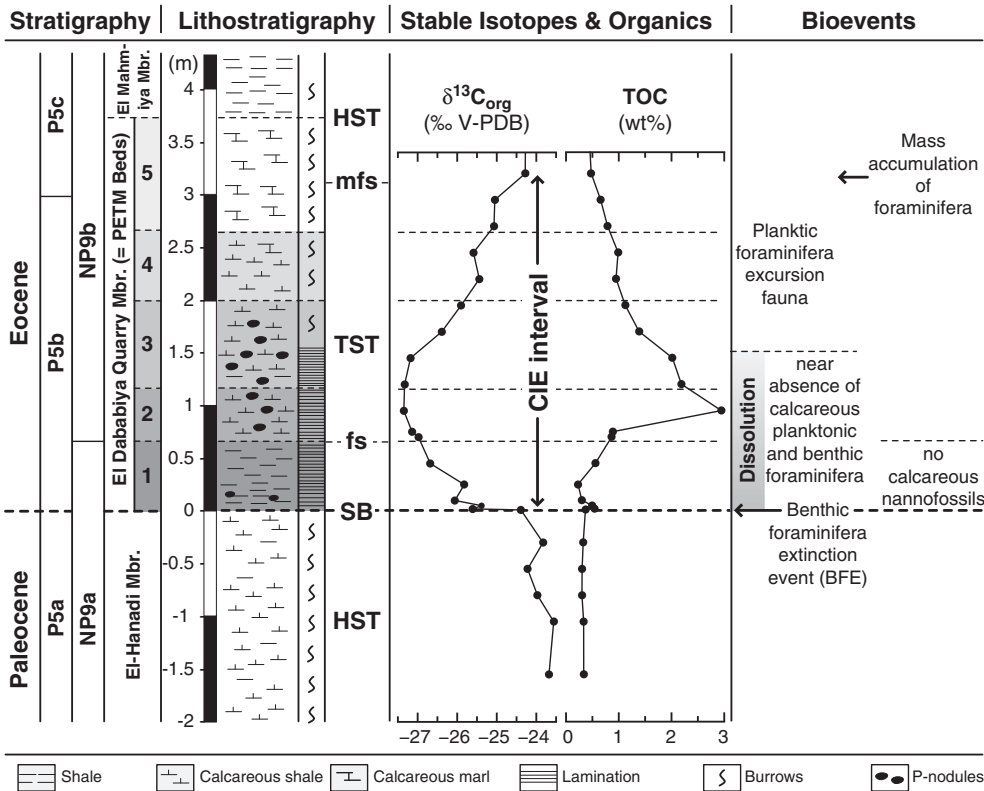


Fig. 4. Litho-, bio-, and isotope stratigraphy of the El-Hanadi Member, the Dababiya Quarry beds, consisting of five beds and the El Mahmiya Member in the section DBH. The GSSP of the base of the Eocene is located at the base of the Dababiya Quarry Bed 1 (Aubry et al., 2007). The sequence stratigraphic interpretation is derived from Speijer and Wagner (2002), Ernst et al. (2006), and data provided in this paper.

### 3. Lithology, paleobathymetry, and organic carbon stratigraphy

The uppermost Paleocene sediments in the Dababiya Quarry belong to the upper Paleocene to lower Eocene Esna Formation and are composed of gray to dark gray shale. The contact between the upper Paleocene El-Hanadi Member and the lower Eocene Dababiya Quarry Member is an erosive unconformity and is positioned approximately 1.8 m above the base of the Esna Shale Formation (see Fig. 4, which also details the biostratigraphic setting as outlined by Dupuis et al., 2003). The Dababiya Quarry Member fills a broad, several hundreds of meters wide channel-like depression. It attains a maximum of 3.7 m in the DBH section and pinches out laterally to less than one meter in the adjacent sections (Dupuis et al., 2003). The Dababiya Quarry Member can be subdivided into 5 distinct beds, the Dababiya Quarry Beds (“DQBEDs”, Fig. 3; Dupuis et al., 2003; Soliman et al., 2006; Aubry et al., 2007). The contacts between these beds are conformable and show no evidence for bioturbation. Individual beds vary in thickness across the outcrops in the Dababiya Quarry area and the thickness for the DBH section is given in parenthesis:

Bed 1 (~0.63 m thick) is a dark gray, non-calcareous laminated shale with very rare phosphate nodules at the base.

Bed 2 (~0.50 m) is a phosphatic brown laminated calcareous shale with numerous phosphate nodules (mainly in the upper part) and some fish debris (spines, teeth).

Bed 3 (~0.84 m) is a brown, laminated phosphatic and calcareous shale with various types of mm to cm-sized, gray to pink colored phosphate nodules and some fish remains (spines, teeth).

Bed 4 (~0.71 m) is a gray calcareous bioturbated shale.

Bed 5 (~1 m) is a prominent light gray calcarenitic marlstone characterized by very high amounts of planktonic foraminifera. The transition to the overlying dark gray shales of the El Mahmiya Member is gradual.

A consistent outer(most) neritic (175 to 200 m water depth) paleoenvironment is inferred based on the presence of common outer neritic and rare bathyal benthic foraminifera species throughout the Dababiya section (Ernst et al., 2006). Only in the lower part of the DQBEDs, benthic foraminifera are almost absent except for very few agglutinated species (Ernst et al., 2006). Based on the analysis of planktonic and benthic foraminifera and by correlation with other PETM sections on the southern Tethyan shelf, a sequence stratigraphic setting across the PETM beds has been assigned (Fig. 4; Speijer and Wagner, 2002; Ernst et al., 2006). Accordingly, the El-Hanadi Member has been considered as representing a (late) highstand systems tract. The DQBEDs have been interpreted as reflecting a transgressive systems tract and their base constitutes a sequence boundary without evidence for subaerial exposure. This assignment is consistent with fully marine settings across the PETM from shallower sections to the southeast (e.g., the Duwi and Aweina sections, Fig. 2; Speijer and Wagner, 2002). The subsequent transgressive systems tract is terminated by a maximum flooding surface that is positioned at the calcarenitic DQBED 5 (Fig. 4).

The stable isotopes of organic carbon across the PETM in the Dababiya Quarry section show the typical magnitude and pattern of the ~3‰ negative carbon isotope excursion (“CIE”) that is observed at many PETM sites globally (Fig. 4; Dupuis et al., 2003; Knox et al., 2003; Magioncalda et al., 2004). The organic carbon content shows peak values of ~3% within DQBED 2 (Fig. 4, Dupuis et al., 2003).

## 4. Results

### 4.1. Bulk rock and clay mineralogy

Our mineralogical results confirm the fluctuations of the phyllosilicate assemblages reported previously (Dupuis et al., 2003; Ernst et al.,

2006), while adding additional details from the bulk rock Rietveld analysis (Figs. 5 and 6A) and the clay mineral analysis of the <2 μm fraction (Fig. 6B). Our results show that the average uppermost Paleocene Esna Formation consists predominantly of illite-smectite (“I-S”), calcite, and quartz (Fig. 5). The I-S shows large full width at half maximum (FWHM) values of >1.5 indicating weak crystallization (Petschick et al., 1996). Additional minor components include kaolinite, chlorite, feldspars, hematite, goethite, jarosite, anhydrite, dolomite, and halite (Fig. 5 and Appendix A).

Prominent mineralogical changes are associated with the DQBEDs. Concurrent with the near absence of carbonates within DQBED 1, two distinct phases of increased detrital input are recorded: An initial phase with slightly increased quartz contents concomitant to strongly increased phyllosilicate contents at the base of DQBED 1; there, the phyllosilicate assemblage is dominated by smectite of beidellitic composition with low FWHM (<0.8) indicating good crystallization. In the overlying part of the DQBED 1, quartz increases and the phyllosilicate contents (mainly weakly-crystallized I-S) gradually decreases. Evidence for a distinct peak in kaolinite abundance at the PETM onset (Bolte et al., 2000b) has not been observed. At the DQBED 1 to 2 transition, the amount of calcium carbonate increases sharply at the expense of the phyllosilicate content, while the quartz content reaches peak values. Grain-size analysis shows that the abundant quartz in this interval is mainly present in the fine-silt fraction (<20 μm). Subsequently, phosphate (present as carbonate fluorapatite, “CFA”) shows peak values of >12 wt.% in beds 2 and 3. Within DQBED 3, the amount of CFA remains high whereas calcite increases significantly and quartz decreases gradually (Fig. 5). This trend is continuing up to DQBED 5 where calcite (calcareous microfauna) shows peak values correlative to the progressive recovery of the carbon isotope values (Figs. 4 and 5).

### 4.2. Major element geochemistry

Since the major element chemostratigraphy reflects mainly the mineralogical changes outlined above and because there is a clear anti-correlation of the Si and Al content with the Ca content, we focus on normalized element/aluminum ratios recording provenance and sediment flux as well as on specific elements (e.g., Fe and S) revealing paleoredox conditions (Figs. 7 and 8; Appendix B). Most elements show major changes at the base of DQBED 1 (Fig. 7) and very high element/Al ratios are recorded during the DQBED 1 to 2 transition for Si, Mg, and K (Fig. 8). Also, there is an extreme increase of the Fe/Al ratio (factor 2.5) and a very high Fe content (up to 12 wt.%) at the DQBED 1 to 2 transition. This increase in iron is difficult to assign solely to a change in the phyllosilicate composition since the smectites have an Al-rich beidellitic composition and the amount of other presumably Fe-rich chlorites in this interval is too low (<6 wt.%) to account for this increase. Remarkably, the element anomalies at the DQBED 1 to 2 transition are paralleled by high sulfur (>2.5 wt.%) contents (Fig. 7). Since the pyrite content as determined by XRD (Fig. 5) is not particularly high during this interval, we consider the sulfur to be primarily derived from anhydrite that is also abundant in this interval (see Fig. 5).

### 4.3. Detritus-characterizing trace elements including REE

Specific trends for the siliciclastic detritus-characterizing elements (e.g., Ti, Zr, and Rb) across the PETM are shown in Fig. 8. Major trends are peak ratios of Ti/Al and Zr/Al within DQBED 1 followed by peak Si/Al ratios at the DQBED 1 to 2 transition. Fig. 9 shows the REE patterns of the DQBEDs normalized to the North America Shale Composite (NASC; Gromet et al., 1984). The REE patterns for the Esna shale and DQBEDs 2 to 5 are generally flat. Major changes in REE composition and abundance are present at DQBED 1 which shows a basal sample that is strongly deprived in REE, whereas the remaining part of this bed reveals a

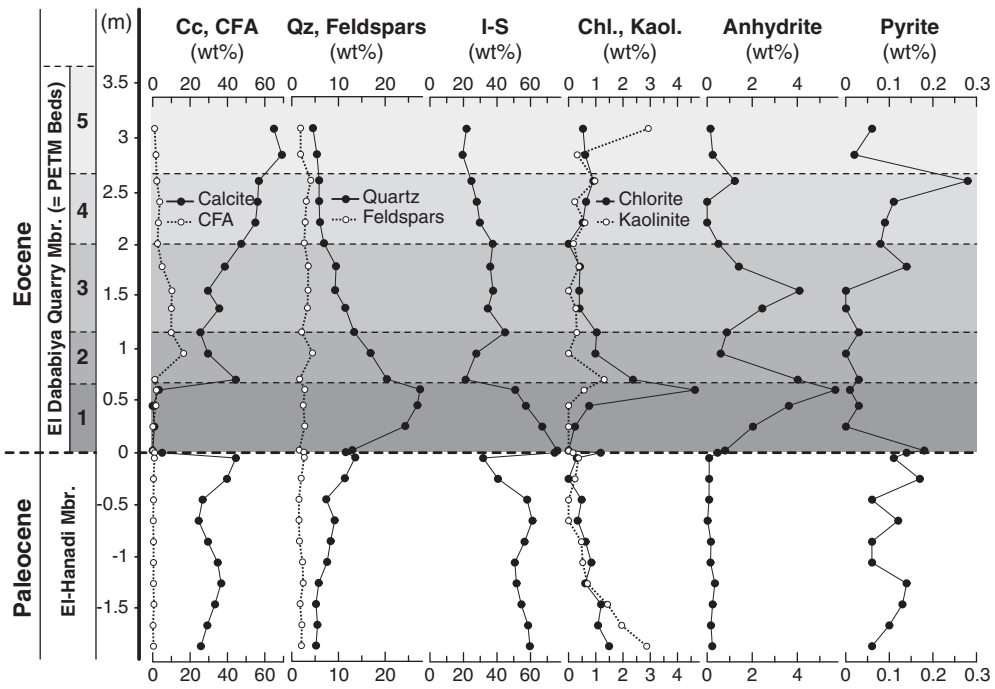


Fig. 5. Bulk rock mineralogical composition based on the results from the quantitative Rietveld analysis. Cc, calcite, CFA, carbonate-fluorapatite; Qz, quartz; I-S, illite-smectite; Chl., chlorite; and Kaol., kaolinite.

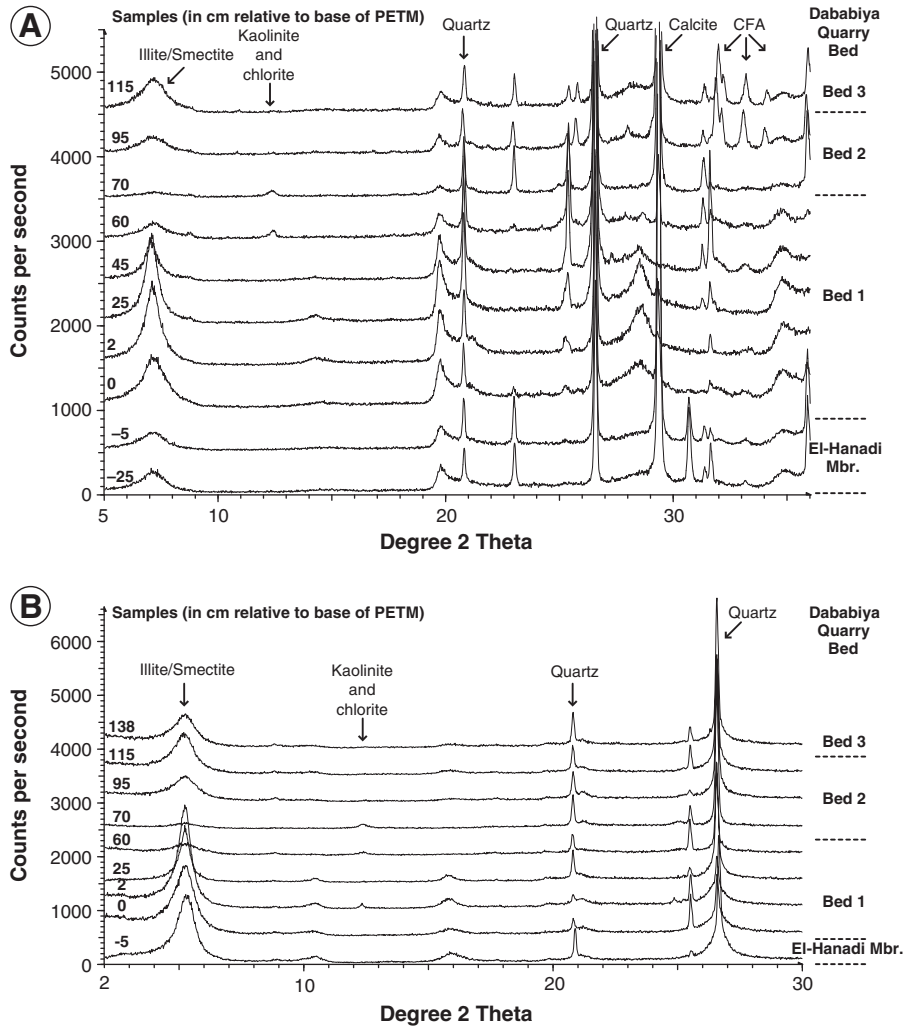


Fig. 6. X-ray diffractometry scans of (A) bulk rock samples (B) the decarbonized and glycolized <2 μm fraction.

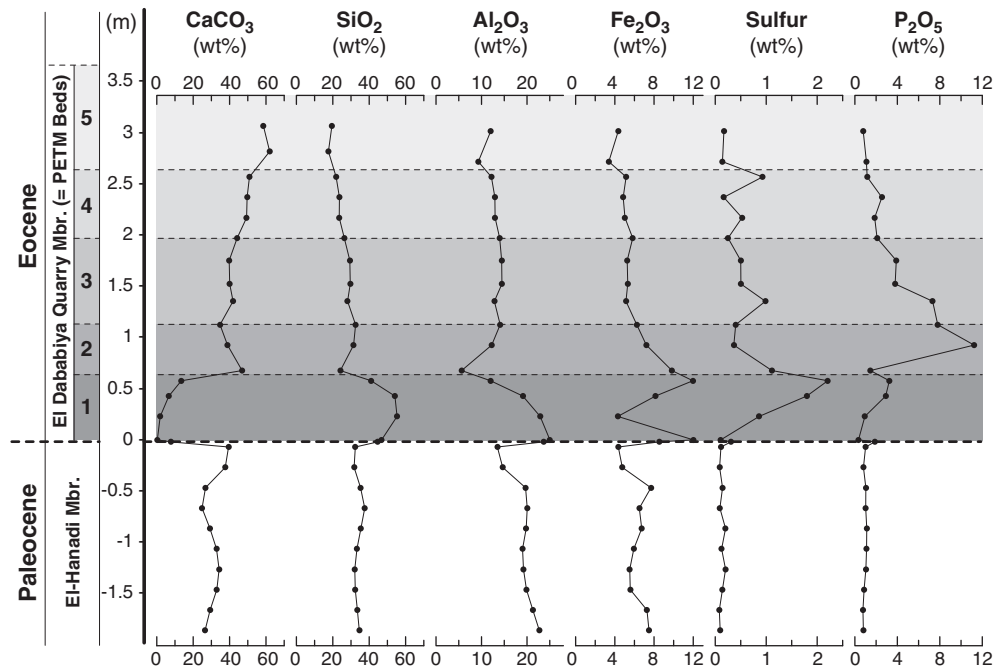


Fig. 7. Selected oxides from XRF analysis to assess changes in the inorganic carbon and siliciclastic flux.

considerable REE enrichment compared to the underlying El-Hanadi Member and the overlying DQbeds.

4.4. Redox-sensitive trace elements

The suite of redox-sensitive trace metals (“TEs”, e.g., Mo, Cu, Ni, As, Cr, and Co) shows a distinct enrichment within the DQbeds that is most pronounced at the DQbed 1 to 2 transition (Fig. 10 and Appendix C and D). To compare the relative enrichment of these elements, we calculated Enrichment Factors (EF) by normalizing each trace element to Al, which is assumed to represent the detrital influx, and comparing these ratios to those of the Esna shale, representing the background

sedimentation (Fig. 10). This approach is commonly used to evaluate redox-sensitive trace element data (e.g., Calvert and Pedersen, 1993; Rimmer, 2004). Accordingly, the Dababiya Quarry Beds exhibit variable, but in part very high (>100-fold) degrees of trace element enrichment. We note, however, that the low Al content of samples from the DQbed 1 to 2 transition which apparently results from a strong quartz enrichment in this interval may have influenced the enrichment factors to a minor degree (less than ~10% reduction). Moreover, the absolute order of element enrichment factors relative to the El-Hanadi Member does not change, being  $\text{Mo, V} \gg \text{Zn} > \text{Ni} > \text{Cr} > \text{Co} > \text{Cu} > \text{Pb}$  at the DQbed 1 to 2 transition, while Mn is depleted within the underlying DQbed 1 (Fig. 10). In Fig. 11, we have complemented the evaluation by

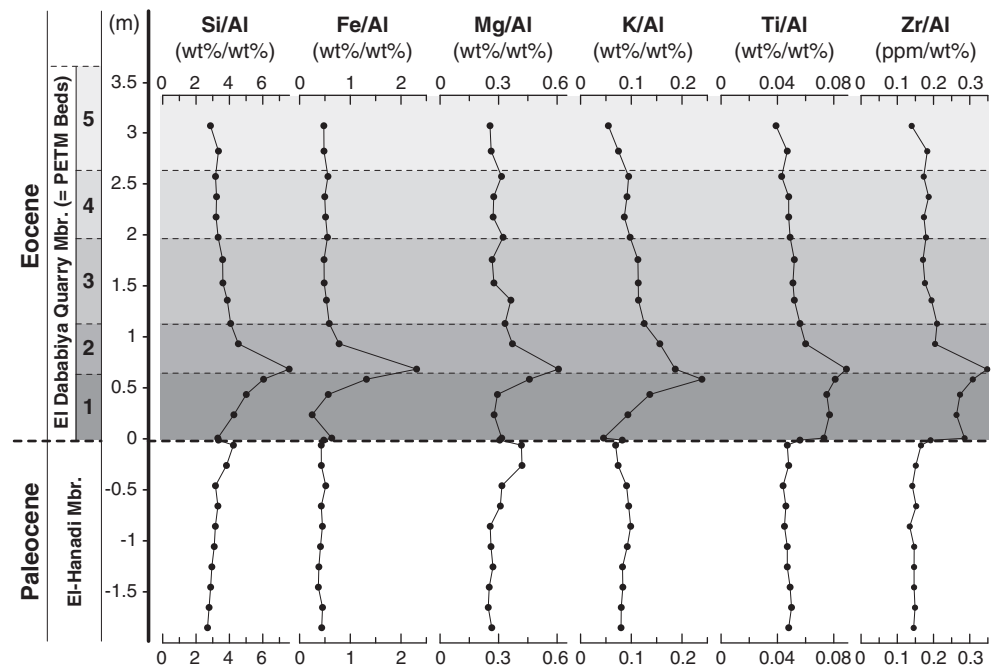


Fig. 8. Selected element/Al ratios from XRF analysis to characterize the detrital fraction.

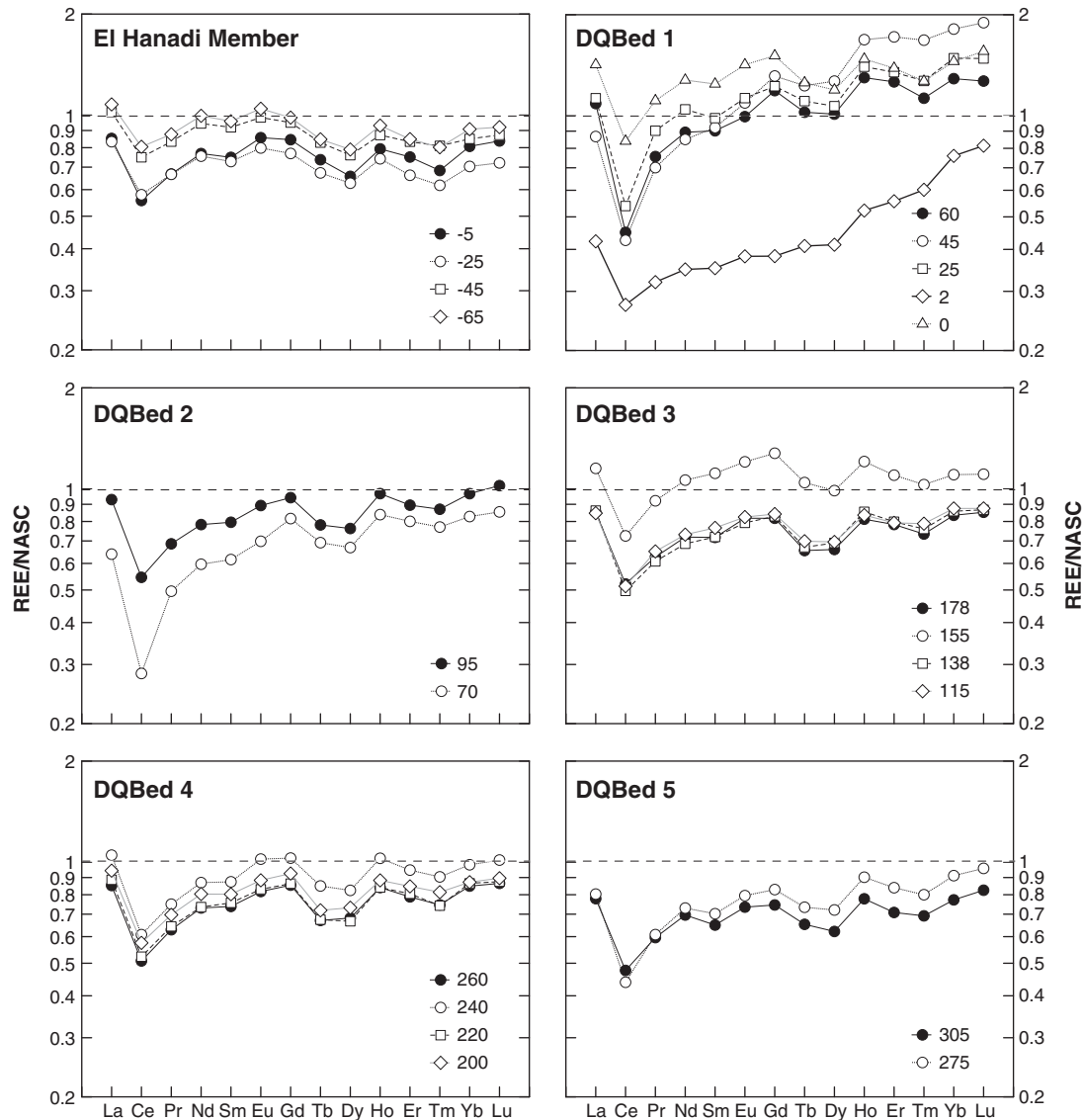


Fig. 9. REE abundances (normalized to NASC values of Gromet et al., 1984) across the PETM in the Dababiya Quarry beds. Sample depths in cm relative to the base of the PETM.

displaying various well-established paleoredox-indices (Jones and Manning, 1994) as well as the Fe/Ti ratio (Werne et al., 2002).

## 5. Interpretation and discussion

Environmental conditions during formation of the DQBEDs were controlled by a number of factors possibly including carbonate dissolution, establishment of anoxic conditions, and sea-level changes. Disentangling the contribution from individual factors during the DQBED formation and later diagenetic and weathering effects, however, requires combining various geochemical and mineralogical proxies, as well as paleontological data.

### 5.1. Diagenesis and weathering

The high abundance of anhydrite as well as iron in the DQBEDs (Fig. 5) is best explained by massive weathering of organic matter- and pyrite-rich sediments associated with conversion of sulfide minerals to sulfates, jarosite, and iron-oxides and -hydroxides (e.g., Littke et al., 1991; Morse and Wang, 1997; Kent and Dupuis, 2003). Anhydrite that frequently occurs in small veins throughout the entire DQBEDs and the enclosing Esna shales (see Plate 1 in Soliman et al.,

2006), probably replaces gypsum because of the current high temperatures and aridity in the Eastern Desert (Kent and Dupuis, 2003). This weathering will also have lowered the original organic carbon content (Littke et al., 1991), as additionally shown by the unusual absence of dinoflagellates in this section (Guasti and Speijer, 2007). A massive weathering overprint and absence of deep burial is compatible with the variable composition and crystallinity of the smectitic minerals (Srodon, 1999; Niu and Ishida, 2000), the regional correlative occurrence of the diverse clay mineral assemblage (Knox et al., 2003), as well as the composition of the organic phases (Dupuis et al., 2003). Thus, a primarily detrital origin of the phyllosilicate assemblages is likely. Considering the effects of weathering on the element geochemistry, especially within the organic-rich intervals of the DQBEDs, previous studies on shale and black-shale weathering have indicated that the influence on immobile TEs (e.g., Ti, Zr, etc.) is generally low, though redox-sensitive TEs are more strongly affected. Nevertheless, some of the redox-sensitive TEs show also a conservative behavior during weathering (e.g., U, V, Ni, Cu; Tribouillard et al., 2006) and the consensus of several studies is that most trace elements that were released during weathering may be fixed within neoformed mineral phases within a few centimeters of their original depth of deposition (e.g., Thomson et al., 1998; Tribouillard et al., 2006; Fischer et al., 2009).

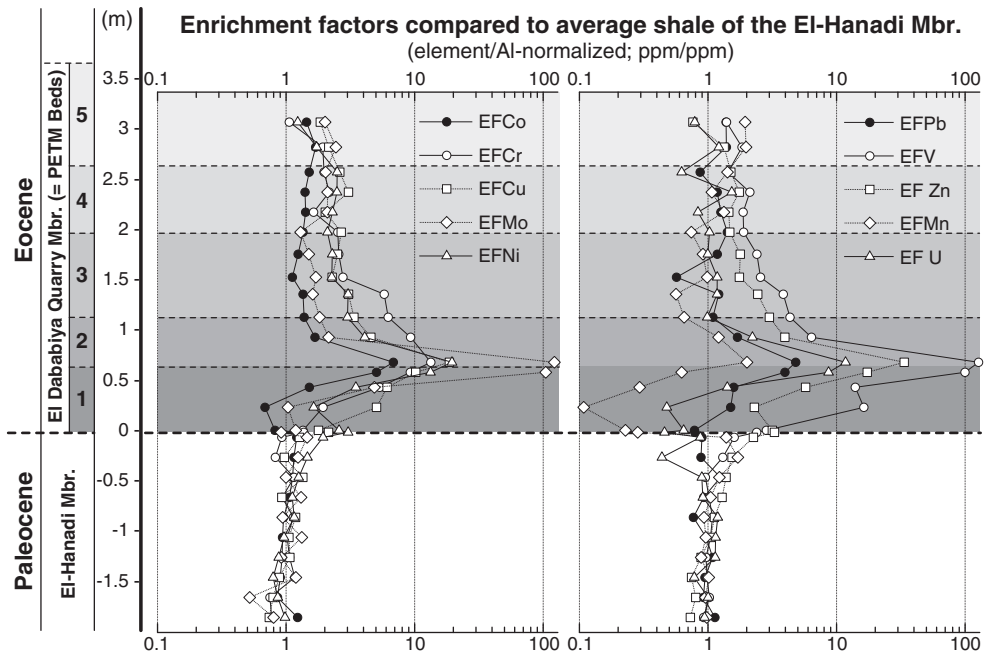


Fig. 10. Compilation of redox indices: (A)  $V/(V + Ni)$  versus  $Ni/Co$  (B),  $V/Cr$  versus  $Ni/Co$ . Ranges for  $V/Cr$  and  $Ni/Co$  redox conditions are from Jones and Manning (1994); ranges for  $V/(V + Ni)$  are from Hatch and Leventhal (1992).

Thus, the geochemical message regarding the sedimentary redox-state is generally preserved.

5.2. Continental weathering and fluvial input: inferences from mineralogy

The illite-smectite phyllosilicate assemblage that dominates in the upper Paleocene El-Hanadi Member and the relatively low kaolinite content suggests influx mainly from alteration products (hydration and

hydrolysis), particularly modified micaceous minerals of basic rocks developed under a variety of climate conditions (Curtis, 1990; Blanc-Valleron and Thiry, 1997; Chamley, 1997; Thiry, 2000). Smectitic soils are generally rare and factors that foster the formation of smectites in soils include low-lying topography, poor drainage, and base-rich parent material (Borchardt, 1989; Thiry, 2000). In particular, smectite-rich vertic soils are often part of catenas comprising kaolinitic soils in the uplands and smectitic soils in low-lying (flood-plain) environments. For instance, kaolinitic soils occur around the inselbergs of the Guéra Range

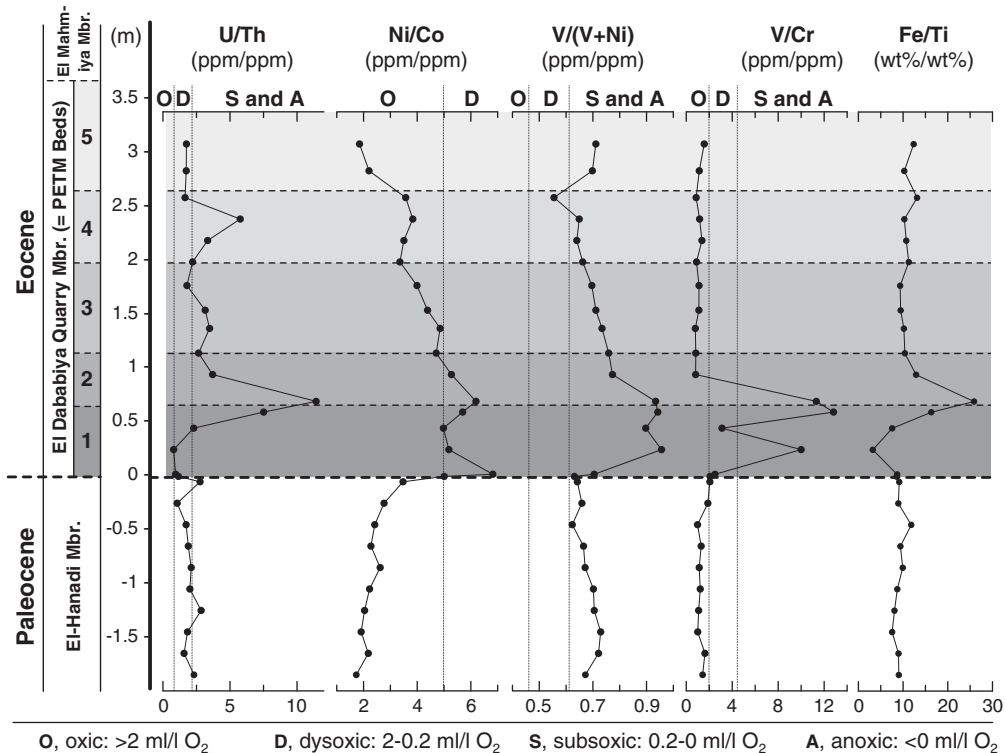


Fig. 11. Enrichment factors of redox-sensitive trace elements normalized to average Esna 1 shale.

in eastern Chad and smectite in the low-lying areas (Thiry, 2000). These low-lying and poorly drained environments are particularly favorable for smectite development under a very broad range of climatic conditions, hindering a straightforward paleoclimatic interpretation of clay mineral assemblages. In addition, on its way to the sedimentary basin, clastic material may transit through such environments and mix with in-situ generated clay minerals, thus clouding the original climatic signal. However, the clay mineral assemblage is consistent with the paleolatitude of 15 to 20°N and prevailing arid conditions with wet seasons in the hinterland during the late Paleocene (Dupuis et al., 2003; Ernst et al., 2006), as also indicated by the general abundance of smectite and the low kaolinite content in the southwestern Tethys margin (Tunisia and Spain), the marginal northeastern Tethys (Kazakhstan), and the Atlantic Realm (northern Spain, Bolle and Adatte, 2001; Schmitz et al., 2001).

The change of the clay mineral assemblage at the base of the DQBEDs, and specifically the high amount of smectite, may have been achieved by increased chemical weathering and an increased hydrological cycle, a shift in the source area, or a change in the fluvial-marine sediment transportation system. Since the time to develop thick soils would probably be too long to explain the very sharp onset of the clay mineral change at the base of DQBED 1 (e.g., Thiry, 2000), we relate the smectite increase to an abrupt change in the source area or transportation system. Consequently, the enrichment in illite-smectite with high crystallinity and less amounts of interstratified illite at the base of the PETM may be explained by several scenarios, including input of altered volcanogenic material or erosion of floodplain deposits.

Although smectites can form from the alteration of volcanic ash, the Paleogene smectites in general and the smectites of the PETM in particular are not considered to result from this process in this study. It has been shown that the Paleogene on the southern margin of the Tethys corresponded to a relatively stable period, without significant hydrothermal or volcanic activity (Charisi and Schmitz, 1995) and volcanoclastic components were not observed in the Dababiya beds by this or other studies (Soliman et al., 2006). Moreover, the trace element pattern of such volcanic ash beds is significantly different from average shale and they are usually very strongly enriched in Zr, Nb, and Ce (Rachold and Brumsack, 2001). There is, however, no extreme enrichment in these trace elements from our geochemical data as outlined below. Thus, the peak in smectite abundance is mostly likely related to detrital input derived from soils.

Increased erosion related to an accelerated hydrological cycle is commonly envisaged to have promoted the peak in detrital influx observed at the onset of the PETM in many sections globally. Paleoclimate models suggest an increase in net evaporation over the subtropical oceans with global warming, reflecting an enhanced hydrological cycle (Bowen et al., 2004; Pagani et al., 2006b). Evidence exists for net evaporation for paleolatitudes up to about 35° N and subtropical high-pressure cells over the eastern Atlantic ocean at 20° to 40° N may have existed, similarly to today (Schmitz and Andreasson, 2001). Consequently, despite global enhancement of the hydrological cycle during the PETM, the tropical to subtropical regions were probably subject to increased seasonality associated with more extreme climate events (e.g., storms). Longer periods of aridity would probably foster less dense vegetation, promoting increased physical weathering, erosion, and runoff (e.g., Schmitz et al., 2001), but not necessarily clay mineral changes. This is similar to the abrupt increase in fluvial detritus input seen in many coastal areas following the human-induced deforestation in recent times (Alt-Epping et al., 2009). For instance, fining-upward sequences found over the entire shelf at the Waipapu River, New Zealand, are interpreted to represent deforestation-induced sedimentation that has overwhelmed the ability of the energetic system to resuspend and segregate fine sediments (Wadman and McNinch, 2008). This interpretation is in agreement with grain-size and mineralogical trends across the PETM from sections on the New Jersey coastal plain, southern Spain, and the Eastern Alps that all are interpreted as reflecting

increased fluvial input and continental erosion rather than neof ormation of clay minerals under more humid climates (Cramer et al., 1999; Schmitz et al., 2001; John et al., 2008; Egger et al., 2009). Therefore, we interpret the peak in phyllosilicate abundance at the very base of the PETM to document an abrupt input of fluvially-derived material that most likely derived from soils in coastal lowland areas. The subsequent brief interval associated with a more diverse kaolinite and chlorite bearing phyllosilicate assemblage at the DQBED 1 to 2 transition may then be explained by an additional shift of the provenance area, tapping landward situated source areas (Dupuis et al., 2003; Ernst et al., 2006) and therefore was likely induced by a sea-level rise.

### 5.3. Continental weathering and fluvial input: inferences from geochemistry

In continental shelf environments, the Si/Al ratio can provide useful information about detrital versus biogenic sedimentation (Dean and Arthur, 1998). In general, Al in shelf sediments is primarily associated with fine-grained siliciclastics derived from fluvial or volcanogenic input, while Si is derived from either fluvial or eolian siliciclastic flux or biogenic flux such as radiolaria or diatoms (Krajewski et al., 1994). In the Dababiya section, major changes of the Si/Al ratio are confined to high peak values at the DQBED 1 to 2 transition, followed by a gradual return to lower values during DQBED 3. Thus, the mineralogical changes (smectite peak abundance) at the base of the PETM apparently do not have a major influence on the Si/Al ratio, but the peak Si/Al ratios at the DQBED 1 to 2 transition need an explanation. Si derived from an additional biogenic Si flux (Werne et al., 2002) could account for this shift and in fact, some hematite-infilled pseudomorphs of radiolarians have been reported for this interval in the Dababiya section (Soliman et al., 2006). However, their abundance in the insoluble residue is fairly low (<20% according to these authors) and they could not be observed in the foraminiferal residues (>63 μm), so they cannot explain the extreme increase of the Si/Al ratio. Also, this anomalous Si enrichment is independent from dilution by carbonate minerals. Therefore, we relate the Si/Al peak rather to the high abundance of quartz concurrent to a low in phyllosilicate abundance reflecting a decrease in the flux of Al (relative to Si) to the shelf. The consistently lower Si/Al ratios of samples from above and below the DQBEDs 1 and 2, which most likely reflect the coupling of Si and Al via deposition of fluvially derived muds, support this conclusion. As shown by scanning electron images of thin sections from the same interval in the Qreiya PETM section (Fig. 4 in Knox et al., 2003), the increased Si/Al ratio is best explained by a relative increase of fine-grained, silt-sized quartz.

Such a marked increase in the Si/Al ratio and quartz content can reflect either a significant climatic shift, i.e. to higher wind strengths or more arid conditions, or condensation due to a decrease in the fluvial supply relative to a constant eolian background flux (Rea, 1994; Wehausen and Brumsack, 1999). The latter scenario would be typical of basin or shelf settings during transgressive to early highstand systems tracts (Werne et al., 2002). Because the change in Si/Al corresponds so closely with other indicators of condensation (such as higher Fe/Al, K/Al, Ti/Al ratios and onset of P accumulation) as well as the increase in organic carbon content, we conclude that the data are best explained by condensation starting at the DQBED 1 to 2 transition. Subsequently, decreasing element/Al ratios indicate a progressive restoration of the normal, fluvially-dominated siliciclastic flux during deposition of DQBEDs 3 and 4.

Additional information on environmental changes may be derived from including the high field strength elements (e.g., Zr, Nb, Hf, and Sc) as well as the rare earth elements (REEs) in our study because these elements are important indicators of provenance area and also reflect various geochemical processes in sediments including sorting, authigenesis, and volcanic or hydrothermal influx (Zwingmann et al., 1999; Jeans et al., 2000; McLennan, 2001; Uysal and Golding, 2003; Zimmermann and Bahlburg, 2003; Setti et al., 2004). Moreover, these

elements are usually immobile and only little affected by weathering and diagenesis (e.g., Utzmann et al., 2002).

Since zircon- and titanium-bearing heavy minerals (e.g., rutile, ilmenite, sphene, and zircon) are generally enriched in sand-silt-sized siliciclastic detritus and Al is generally enriched in the clay-size fraction (Fralick and Kronberg, 1997; Dypvik and Harris, 2001), we suggest that the very high Zr/Al and Ti/Al ratio at the very base of DQBed 1 (Fig. 9) document a brief influx of more coarse-grained sediments, analogous to a ravinement surface (Cattaneo and Steel, 2003). Subsequently, at the DQBed 1 to 2 transition, the significantly higher Mg/Al and K/Al ratios, and second peak of the Ti/Al and Zr/Al ratios corroborate the conclusion of condensation in this interval outlined above and correspond well with the relatively higher input of illite (K-rich) and chlorite (Mg-rich) from less-well weathered crystalline source rocks (Cox et al., 1995) by fluvial or eolian transport. Subsequently, during deposition of DQBeds 2 and 3, the Ti/Al ratios (as well as the K/Al, Zr/Al, and Rb/Al) ratios are still elevated compared to the Esna shales before reaching background values within DQBeds 4 and 5. The same applies to the quartz content, which also shows elevated, albeit decreasing values during this interval. In concert, this suggests that the provenance area tapped during the rapid sea-level rise still delivered sediment to the Dababiya area until deposition of DQBed 3, albeit at much lower quantities.

Considering the distribution pattern of the REEs, the North America Shale Composite (“NASC”; Gromet et al., 1984) normalized Esna shales show a relatively flat pattern, suggesting a detrital origin and good mixing during transport (Fig. 9). There is only a slight decreasing trend of the La/Yb ratio – which is generally used to show the depletion of the light REE with respect to the heavy REE. The presence of a negative Ce anomaly in all samples supports a high water–rock ratio diagenetic system typical for marine sediments. The good correlation between Nd and major elements (e.g., Al) indicates that for the El-Hanadi Member, the REEs are probably located in clay minerals.

Considerable changes in relative REE abundance occur within the lowermost DQBeds (Fig. 9). Except for one sample from the very base of DQBed 1, which shows a strong depletion in REEs, all other samples from DQBed 1 show a significant REE enrichment compared to the enclosing lithologies and also an enrichment of heavy REE relative to light REE. The general high abundance of REEs in DQBed 1 attests to the large amount of fine-grained siliciclastic input (McLennan, 2001). The slight increase in heavy REE, as also indicated by the higher La/Yb ratio may be explained by the observation that a large part of the heavy REE in the siliciclastic fraction may be bound to heavy minerals (e.g., zircon and monazite).

The strong depletion in REE in one sample from the very base of the DQBed 1 may be explained by a brief influx of sediments depleted in REE relative to the shales of the El-Hanadi Member. However, from the mineralogical and geochemical data, there is no evidence for a major change in sedimentary composition other than the total lack of carbonate in this sample and an increase in smectite abundance. Moreover, the mineralogical composition appears to be very similar to the enclosing samples, which show no distinct REE depletion. Therefore, an alternative explanation for the REE depletion at the very base of the DQBeds incorporates acidic pore waters. Experiments showed that weak acidic, CO<sub>2</sub>-saturated water releases large amounts of REE from clay minerals that are then transported as carbonate complexes (Brookins, 1989). Specifically, smectites with their high cation exchange capacity are prone to REE loss. Therefore, we speculate that a brief phase of sea-floor acidification during the onset of the PETM may be one explanation for this “negative REE anomaly” that would also account for the complete absence of calcite in the basal part of DQBed 1. A prominent carbonate dissolution interval characterizes the onset of the PETM in most open ocean and shelf sites (e.g., Sluijs et al., 2007). In shelf sections, the effects of corrosive waters and dissolution may have been enhanced by dilution of carbonates by the strong and abrupt increase in the supply of terrigenous silicious detritus and refractory organic

matter at the onset of the PETM, as outlined before (e.g., Schmitz and Pujalte, 2007; John et al., 2008; Alegret et al., 2009). Nevertheless, increased detritus input hardly accounts for the observed total absence of carbonate at the base of the PETM and lateral advection of corrosive waters onto the shelf may explain the abrupt onset of intense carbonate dissolution observed at the Dababiya section and at many other localities in the Tethyan realm, considering a pulse-like release of large quantities of CO<sub>2</sub> into the ocean–atmosphere system at the PETM onset (Zachos et al., 2005).

#### 5.4. Redox history across the PETM

The DQBeds 1 to 4 are, in part, considerably enriched in redox sensitive and/or sulfide forming TEs, including Mo, U, V, Zn, Co, Cu, Cr, Pb, and Ni. While Ni and Cu are also possible indicators of the OM flux to the sediments, these TEs can be fixed in high amounts in sediments under reducing conditions (e.g., Calvert and Pedersen, 1993; Lipinski et al., 2003; Algeo and Maynard, 2004; Meyers et al., 2005; Brumsack, 2006; Tribovillard et al., 2006). They may be precipitated as sulfide phases (Co, Zn, and Pb), coprecipitated with iron sulfides (Mo, V, Ni, and Cu), and/or bound to organic matter (V, Mo, Ni, Cu, and U). However, several TEs may show strong detrital influence (Cr and Co) or are highly mobile during post-sedimentary diagenesis or weathering (Zn and Pb; Tribovillard et al., 2006). Therefore, we focus mainly on the U, V, Mo, Ni, and Cu enrichment patterns since these TEs are considered to be the most reliable paleoredox indicators which are least vulnerable to diagenetic and weathering effects (Tribovillard et al., 2006). The evolution of the TE enrichment within the DQBeds suggests normal, oxygenated conditions during deposition of the El-Hanadi Member and a gradual onset of oxygen-deprivation during DQBed 1 deposition, as shown by low to moderate TE enrichment factors (Fig. 10). Subsequently, the DQBed 1 to 2 transition reveals an extreme TE enrichment (particularly in Ni, Cu, and Mo; Fig. 10), and, as shown by the concurrent strong enrichment of U and V, reflects a brief period of fully anoxic and most likely euxinic conditions at the sediment–water interface or in the water column (Algeo and Maynard, 2004). During deposition of DQBeds 2 and 3, TE enrichment factors drop considerably, indicating improved oxygenation although ventilation of the seafloor may have been only brief and intermittent (e.g. seasonal), as suggested by Speijer and Wagner (2002). Finally, TE enrichment factors drop to background values within DQBeds 4 and 5, suggesting that normal oxygenation like before the PETM was restored.

A comparison of these interpretations with evidence derived from characteristic redox ratios, including the Th/U, Ni/Co, V/Cr, and V/(V + Ni) ratio is shown in Fig. 11. All these redox proxies (except for the Th/U ratio) reveal variable, though generally oxygen-deprived conditions for the DQBeds 1 and 2. Except for the very base of the DQBed 1 as outlined above, there is a fairly good agreement between the various trace metal ratios used as redox proxies that are all indicative for oxygen-deficiency with lowest oxygen concentrations at the DQBed 1 to 2 transition: anoxic-dysoxic (Th/U), dysoxic (Ni/Co), and anoxic (V/Cr and V/(V + Ni)).

Besides the strong enrichment of TEs with strong euxinic affinity (Mo, U, V, and Zn; Lyons and Severmann, 2006; Algeo and Maynard, 2004; Paillard, 2001) at the DQBed 1 to 2 transition (Fig. 10), additional evidence for a distinction between anoxic and sulfidic (euxinic) settings may derive from geochemical proxies including the Fe/Al, Fe/Ti, and the Mo/Ti ratio (Werne et al., 2002; Lyons and Severmann, 2006). Although high degrees of weathering, as observed in the Dababiya section, result in mineralogical changes that repartition the elemental constituents, the total amount of Fe, Ti, and Mo should remain constant despite any internal redistribution (Lyons and Severmann, 2006). Specifically, the decoupling between the Fe and the Al and Ti delivery, as revealed by strongly elevated Fe/Al (Fig. 8) and Fe/Ti (Fig. 11) ratios, is consistent with a brief period of iron scavenging from a euxinic water column during syngenetic pyrite formation and deposition in the underlying sediments (e.g., Lyons and Severmann, 2006). Such an iron augmentation is not only decoupled from the local biogenic sediment flux (Canfield et

al., 1996), but also takes place under a comparatively low siliciclastic flux (i.e. condensation; Werne et al., 2002), and it does appear to be a uniquely euxinic phenomenon (Lyons and Severmann, 2006). Similarly, the Mo/Ti ratio as well as the Mo/Al ratio (not shown) records an extreme increase at the DQBed 1 to 2 transition, suggesting very rapid development of sulfidic conditions in the water column coupled with a decrease in detrital dilution, and hence improved exchange between bottom waters and pore waters (Werne et al., 2002).

It is remarkable that the level showing the highest enrichment in TEs outlined above exhibits only a fairly low organic carbon content of about 1% while the overlying DQBeds 2 and 3 (lower half) show significant higher organic carbon content, albeit much lower TE enrichment factors. This less pronounced correlation of the TE enrichment with organic carbon may be explained by post-sedimentary bacterial degradation and weathering of organic matter, specifically affecting sediments at the DQBed 1 to 2 transition with an originally high pyrite content. In addition, under euxinic conditions, in which free hydrogen sulfide is present and trace elements are generally reduced to their lowest valence state, insoluble metal sulfides and oxyhydroxides can precipitate in large quantities directly from the water column or at the sediment-water interface. These conditions may have resulted in the strong U and V enrichments and weak correlations with the total organic carbon contents observed at DQBed 1 to 2 transition, because Mo, U, and V reside mainly in authigenic mineral phases rather than organic phases (e.g., Algeo and Maynard, 2004).

## 5.5. Depositional scenario

### 5.5.1. Onset of the PETM

The onset of the PETM succession in the Dababiya section (DQBed 1) is characterized by an abrupt shift to peak phyllosilicate deposition infilling broad channel-like depressions which probably formed during a relative sea-level fall immediately preceding the PETM (Fig. 12A and B). Although bathymetric estimations based on benthic foraminifera are not available for the lower part of the DQBbeds, lithological changes and microfossil assemblages from the nearby Duwi PETM section in eastern Egypt suggested that during the ~60 ky period prior to the PETM, relative sea level fell by ~15 m (e.g., Speijer and Morsi, 2002; Speijer and Wagner, 2002). Subsequently, sea-level started to rise concurrent to the onset of deposition of the PETM event beds. The pulse in detrital material and shift in phyllosilicate assemblages within DQBed 1 suggests that low-lying flood-plain deposits and soils rich in well-crystallized smectite were eroded, eventually filling-up the channel structures on the shelf either during the sea-level lowstand or during the early sea-level rise. Nevertheless, a transgression combined with a strong input of siliciclastic material during the onset of the PETM is in contrast to existing sequence stratigraphic models. Although it is clear that a rapid sea level rise can provide increased accommodation space (John et al., 2008), it is usually underfilled during the transgression since the landward shoreline migration over a wide area increases the sedimentation area, lowering net sedimentation rates. This applies specifically to the low-gradient ramp-type settings encountered on the southeastern Tethyan shelf. Therefore, transgressive deposits in settings away from the basin margin and the shore-connected sediment prism are normally relatively thin compared to lowstand and highstand systems tracts deposits (Cattaneo and Steel, 2003; Zecchin, 2007). Solving this conundrum requires that the increasing distance to the shoreline was outpaced by a progressive increase of detrital (fluvial) input and erosion of coastal areas. Hence, the erosion of floodplain areas and soils, and the terrestrial discharge must have strongly increased during the onset of the PETM.

Another important characteristic of the PETM record in the Dababiya section is the evidence for an abrupt onset of oxygen-deficiency within DQBed 1 (Fig. 12B) as shown by absence of benthic fauna and sediment lamination. However, a marked TE or organic carbon enrichment is confined to the top of this bed as outlined below. This decoupling of

sedimentary versus geochemical proxy data suggests that elevated productivity may not be the cause for the oxygen-deprivation and other mechanisms have to be considered.

One depositional scenario for the onset of oxygen-deficiency would include lateral advection of oxygen-depleted water from the Tethyan Ocean (Speijer and Wagner, 2002). In fact, recent reports from PETM sites in the Pacific suggested that the absence of bioturbation at the base of the PETM records a phase of hypoxia probably caused by an expansion and intensification of an OMZ (e.g., Nicolo et al., 2010). Moreover, an expanding OMZ encroaching into the epicontinental southern Tethyan basins would explain similar observations from PETM sites in Sinai and on the northern part of the Egyptian shelf.

Another explanation for the onset of oxygen-deficiency involves the development of a thick suboxic zone on the extensive Egyptian epicontinental shelf. A stable water column stratification associated with a thick suboxic zone could be triggered by the higher sea surface temperatures and increased amount of fluvial freshwater discharge during the PETM onset. Although there is no evidence for the development of a freshwater lid extending across the Egyptian shelf, a high fluvial input is basically supported by our mineralogical data. A similar high fluvial discharge conducive to the evolution of a suboxic zone has been suggested for the Atlantic Coastal Plain, which shows an abrupt shift to clay-sized sedimentation at the base of the PETM (e.g., Cramer et al., 1999; John et al., 2008; Kopp et al., 2009). Moreover, in the modern world, some of the thickest suboxic zones occur in tropical river-dominated continental shelves like the Amazon Shelf (Aller, 1998) and the Gulf of Papua (Aller et al., 2004), and we suggest that analogous environmental conditions developed during the PETM.

### 5.5.2. Peak phase of the CIE

Peak negative values of the carbon isotope excursion are present around the transition from DQBed 1 to 2 and correspond to the onset of a pronounced organic and inorganic carbon enrichment and anoxic (likely euxinic) conditions as well as to an abrupt decrease in the amount of phyllosilicates relative to quartz (Fig. 12C). As shown by our mineralogical and geochemical data, this change in the detrital composition is not a simple dilution effect due to the increase of calcium carbonate in this interval, but most likely reflects a reduced detrital influx (condensation) as the result of a rapid sea-level rise. Although paleobathymetric data from benthic foraminifera are not available at Dababiya to support this, a rapid sea-level rise of up to 20 m has been proposed for the peak phase of the PETM from the Gebel Duwi section (Fig. 2; Speijer and Morsi, 2002). Similarly, studies from the Tethyan margins (Speijer and Wagner, 2002; Gavrillov et al., 2003) and from the New Jersey continental shelf indicated that a transgressive pulse occurred at the onset of the PETM (Gibson et al., 1993; Cramer et al., 1999; John et al., 2008; Sluijs et al., 2008).

Possible mechanisms for explaining the rapid PETM sea-level rise may have been the thermal expansion of the seawater due to global warming at the PETM. However, the amplitude of thermally-induced eustatic sea-level rise (5 m due to the average 5 °C warming of the oceans; Speijer and Wagner, 2002; Sluijs et al., 2008) is considered too low to account for the observed rise of about 20 m. Therefore, either glacioeustasy, incorporating melting of small ephemeral ice sheets in the Antarctic (Miller et al., 2005) and emplacement of the North Atlantic Igneous Province associated with rapid submarine uplift (Storey et al., 2007) are currently discussed as additional mechanisms. Their combined effects may explain the magnitude of sea-level rise observed during the PETM (Speijer and Morsi, 2002; Speijer and Wagner, 2002; Sluijs et al., 2008).

The rapid sea-level rise outlined above affecting the low-gradient broad, epicontinental Egyptian shelf would result in considerable displacement of the shoreline during the onset of the PETM. Our proxy data is basically in agreement with these studies and suggests a flooding event correlative to the DQBed 1 to 2 transition. Such a close association of sediment starvation and the formation of black shales

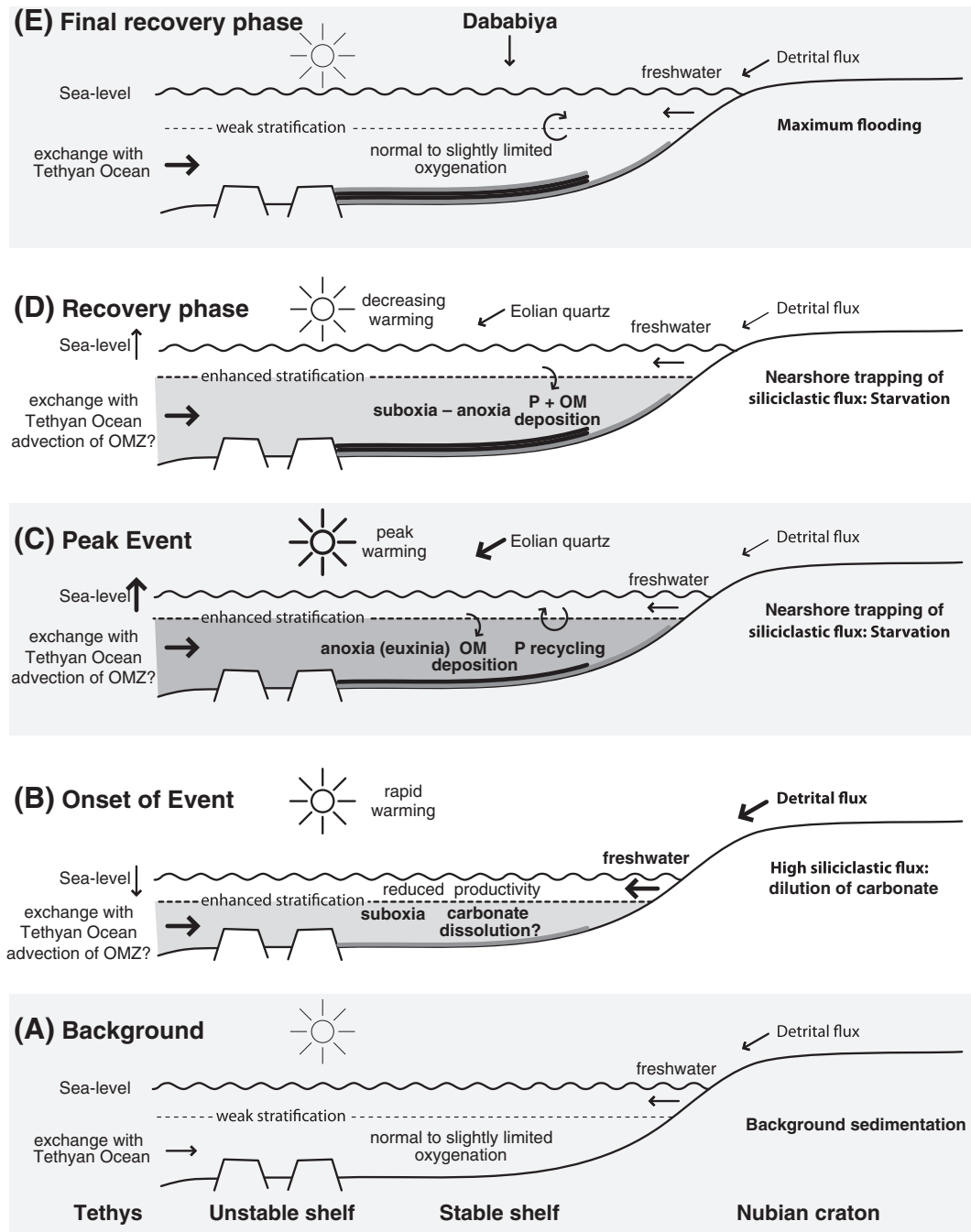


**Fig. 12.** Conceptual model of environmental changes across the PETM in a transect across the southern Tethyan shelf as explained in the text. (A) Background conditions, (B) onset, (C) peak phase, (D) early recovery phase, and (E) late recovery phase of this hyperthermal event. Paleogeographic setting based on Speijer and Wagner (2002).

strongly suggest a causal connection and in fact, such thin intervals of black shales are frequently linked to transgressive settings in the geological record. Prominent examples are the late Jurassic black shales from the Boulonnais in northern France (Wignall and Newton, 2001; Tribouillard et al., 2004). In this study, the formation of transgressive black shales was explained by the position of the thermocline at a deep level, thereby allowing basin margin euxinic to develop due to less frequent overturning by storms, although it is, still unclear why these specific conditions are related to the initial phase of transgressions (Wignall and Newton, 2001). For Middle Devonian black shales in the Appalachian basin, Werne et al. (2002) pointed out that a number of different factors contributed to the deposition of organic carbon-rich black shale, but that the ultimate controlling factor was a relative sea-

level rise. There, concurrent with the shift to dominantly euxinic conditions during the transgression, the supply of siliciclastic sediments was cut off, resulting in sediment starvation (condensation). Based on our mineralogical and geochemical data, this is a situation that is very similar to the onset of enhanced organic carbon deposition and anoxic (euxinic) conditions in the Dababiya PETM section. By analogy, we suggest that once a threshold was crossed, sediment starvation on the Egyptian shelf may have facilitated the biogeochemical (re)cycling of C and P (Glenn and Arthur, 1990; Bruland et al., 2005). Specifically the preferential regeneration of P under anoxic conditions may have led to enhanced primary production in surface waters, thereby maintaining euxinic conditions in the bottom waters through respiration of settling organic matter.

Moreover, recent studies of anoxia developing in the northern Gulf of Mexico area (e.g. Rabalais et al., 2009) suggest that the decreasing area (and reworking) of coastal lowlands, wetlands and floodplains due to a sea-level rise will not only increase nutrient discharge but also enhance the release of organic matter to the shelf. Today, these areas are important ecosystems because they play a pivotal role in the removal of reactive nitrogen (Galloway and Cowling, 2002). Further factors promoting surface productivity and oxygen-deficiency were likely elevated sea-surface temperatures as well as enhanced fluvial runoff. Although peak temperatures and surface runoff may have already been declining following the light carbon release at the CIE onset, it is likely that these parameters were still elevated compared to pre-PETM background values. However, it is certainly beyond the scope of this paper to evaluate all of these mechanisms in detail. In agreement with a number of studies on ancient and modern black shale depositional systems, it is likely that the onset of anoxia and OM deposition was likely a combination of several “adverse” mechanisms (e.g., warming, increased weathering, and stratification) with one important controlling factor on the Egyptian shelf being sea-level rise. A similar conclusion was drawn from studies of PETM black shales from other Tethyan regions (Bolte et al., 2000a; Gavrilo et al., 2003) and the Antarctic (Sluijs et al., 2006). There, a sea-level rise concomitant to elevated nutrient input and fluvial discharge were the major factors promoting accumulation of organic carbon and development of anoxic and euxinic conditions.

In concert these results strengthen our conclusion that sea-level change was an important variable in determining carbon burial during the PETM. Although a detailed quantification of the carbon flux is currently not available, upon considering the large shelf areas covered by black shales, we suggest that sea level rise may have been an effective feedback mechanism triggering carbon sequestration during the PETM.

#### 5.5.3. The early recovery phase of the PETM

The PETM recovery interval (DQbeds 2 and 3) is characterized by high organic carbon and high phosphorite contents in concert with evidence for oxygen-deficiency (lamination, elevated content of redox-sensitive TEs, and near absence of benthic organisms). Such characteristics are usually typical for sediments beneath upwelling zones (e.g., Smith, 1992; Summerhayes et al., 1995; Bruland et al., 2001). Accordingly, previous studies on Tethyan PETM sections concluded that the ultimate driving force behind the origin of the phosphorite-rich PETM beds is the stimulation of primary productivity by upwelling of nutrient-rich intermediate Tethyan water into the epicontinental basin (e.g., Speijer and Wagner, 2002; Soliman et al., 2006). Upwelling of Tethyan intermediate water masses would have started at the onset of the recovery interval (base of DQbed 2) and ended during the recovery phase (at about DQbed 4), comprising an interval much shorter than the total duration of the PETM (~170 ky, Röhl et al., 2007).

On the other hand, such phosphate-rich beds are rarely encountered in Paleogene sediments from Egypt. After a climax in phosphorite deposition during the Campanian, phosphate accumulation ceased rapidly during the Maastrichtian and subsequently, during the early Paleogene, the loci of upwelling and phosphogenesis shifted to the Northwest African margin (e.g., Soudry et al., 2006). The shift of the upwelling areas is well reflected by  $\epsilon\text{Nd}(T)$  compositions in the Middle East and North African phosphorites and may have resulted from the gradual plate-tectonic closure of the Tethys seaway and the concurrent progressive widening of the Atlantic Ocean (e.g., Soudry et al., 2006). Both tectonic events probably resulted in a restriction of the Tethyan circumglobal current and the start of upwelling along the Northwestern African margin driven by the Atlantic (Soudry et al., 2006). Consequently, besides the PETM beds and the Latest Danian Event bed (e.g., Speijer, 2003; Bornemann et al., 2009), no distinct phosphorite beds have been recognized in Paleocene–Eocene sediments from Egypt (e.g., Tantawy et al., 2001). Moreover, today's continental-margin upwelling

regions occupy very localized, narrow zones on the shelf, no more than 10 to 50 km wide and close to the coastline (Glenn and Arthur, 1990), and tend to exhibit patchy concentrations along a linear trend (e.g., Smith, 1992; Glenn et al., 1994; Summerhayes et al., 1995). In contrast, the Egyptian phosphorite-rich PETM beds are correlative over large distances (e.g., to the eastern Desert; Scheibner et al., 2005; Speijer and Wagner, 2002) and their location is removed from the open Tethyan Ocean by several hundred kilometers, providing an unusual long pathway for upwelling waters (Fig. 2; Gheerbrant and Rage, 2006). Also, the localized presence of topographic swells on the Syrian Arc (unstable shelf) may have been obstacles for inflowing Tethyan waters (Salem, 1976). Consequently, we suggest that upwelling is rather unlikely to account for the formation of organic carbon and phosphorite-rich beds during the recovery interval of the PETM.

Further clues to the origin of the phosphate-rich beds may be derived by constraining conditions for the formation of such beds. Generally, the burial efficiency of P increases when bottom waters become progressively more oxic due to redox-dependent changes in iron phases carrying P as well as due to microbial activity (Van Cappellen and Ingall, 1994, 1996). Thus, following the peak of anoxic conditions at the DQbed 1 to 2 transition, the siliciclastic influx ceased and Fe–P-recycling would have been diminished concomitant to improved oxygenation of the bottom waters during deposition of DQbeds 2 and 3 as indicated by the considerably lowered TE enrichment factors compared to the underlying interval. This switch to at least intermittently improved oxygenation allowed for P removal in the water column and deposition at the sea floor. In concert with similar observations of phosphorite occurrences in the eastern Tethys (e.g., Gavrilo et al., 2003), the southern Tethyan shelf area may have become an important reactive P sink during this phase of the PETM.

Generally, and analogous to the formation of black shales, phosphorite genesis is frequently linked to changes in sea level and many major phosphorite accumulations are correlated with marine transgressions (e.g., Glenn and Arthur, 1990; Glenn et al., 1994; Föllmi, 1996). Specifically, transgressive episodes may favor phosphorite accumulation by restricting the locus of diluting siliciclastics in a landward direction (sediment starvation, Glenn et al., 1994). This explanation is in good agreement with the quartz abundance and high Si/Al elemental ratios for this interval as outlined above. Moreover, the presence of well preserved fish debris and large phosphate nodules in the DQbeds 2 and 3 (see also Soliman et al., 2006) are typical for phosphate accumulation during such condensed sections (Glenn et al., 1994).

#### 5.5.4. The late recovery phase of the CIE

Finally, during the late recovery phase of the CIE represented by the DQbeds 4 and 5, the siliciclastic flux has not returned to pre-event values. Although the quartz ratio has dropped to values comparable to the El-Hanadi Member underlying the Dababiya Quarry beds, the phyllosilicate contents is still significantly lower. If our interpretation of strongly elevated quartz contents as being indicative for extreme condensation is correct, the return to background values would suggest restoration of normal sedimentary conditions. The concurrent drop in sedimentary evidence for TE, organic carbon, and phosphate enrichment as well as the reappearance of burrowing suggest a causal connection between cessation of condensation and improved seafloor oxygenation. However, the carbonate content is considerably higher than in the strata preceding the PETM. Excess carbonate sedimentation during the late PETM recovery has been observed in a number of PETM sites (e.g., ODP Site 690; Röhl et al., 2000) consistent with the suggestion of a supersaturated ocean (Farley and Eltgroth, 2003; Kelly et al., 2005; Röhl et al., 2007). Likewise, in the southern Tethyan shelf sections, this excess carbonate sedimentation may reflect the lower siliciclastic input during a maximum flooding phase on the shelf (e.g., Speijer and Wagner, 2002).

## 6. Conclusions

Our multi-proxy mineralogical–geochemical investigation of the PETM event beds in the Dababiya Quarry revealed the following succession of environmental changes:

- (i) At the very base of the PETM event beds, the virtual absence of carbonate and strong deprivation of REEs may indicate a brief period of severe carbonate dissolution, possibly reflecting leaching by corrosive waters. A concurrent sharp increase in siliciclastic detritus and peak abundances of phyllosilicates suggest deposition during low or rising sea-level and increased fluvial input. A switch from illite-smectite to well-crystallized smectite is consistent with erosion of low lying coastal areas. The absence of lamination combined with absence of a pronounced organic carbon or TE enrichment may reflect either the development of a suboxic zone or OMZ expansion onto the shelf.
- (ii) During the peak phase of the PETM, i.e. during the maximum negative shift of the CIE, a short-lived period of anoxic and likely euxinic conditions developed as indicated by an elevated organic carbon content and the extreme enrichment in redox-sensitive TEs and iron. The enrichment of the TEs relative to the background Esna shale is  $Mo \approx V \gg Zn > Ni > Cr > Co > Cu$ . Very high Fe/Al, Fe/Ti, and Mo/Ti ratios and the high Fe content of this bed indicate decoupling of the iron flux from the siliciclastic flux during euxinic conditions in the water column. These conditions may have resulted from rapidly rising sea level and condensation, which is evident from the increase in the relative concentration of Si versus Al and the increase in quartz content.
- (iii) Sediments from the recovery phase of the PETM are characterized by a strong phosphate and organic carbon enrichment (up to 12 wt.% and 3 wt.%, respectively). During this phase, TEs are still enriched, albeit at a lower level compared to the preceding phase, indicating at intermittent (seasonal?) ventilation of the seafloor. Finally, bioturbation resumed indicating more or less continuous ventilation of the seafloor.

We suggest that the formation organic carbon- and phosphate-rich sediments during the peak phase of the PETM supports current views that shelf areas acted as large carbon and P sinks. Oxygen-deficiency coincided with sea-level rise and was probably sustained by the significant warming, an elevated freshwater and detrital flux, and enhanced water column stratification.

## Acknowledgments

P.S. thanks the Herta and Hartmut Schmauser Stiftung from the University of Erlangen for support. The K.U.Leuven Research Fund is acknowledged for financial support to R.P.S. We thank Stefan Krumm, University of Erlangen, for help with the X-ray diffractometry and calibration as well as Michael Joachimski, University of Erlangen, for discussions. We are also grateful to two anonymous reviewers for valuable comments.

## Appendix A. Supplementary data

Supplementary data to this article can be found online at doi:10.1016/j.chemgeo.2011.04.004.

## References

Alegret, L., Ortiz, S., Orue-Etxebarria, X., Bernaola, G., Baceta, J.I., Monechi, S., Apellaniz, E., Pujalte, V., 2009. The Paleocene–Eocene thermal maximum: new data on microfossil turnover at the Zumaia section, Spain. *Palaios* 24, 318.

Algeo, T.J., Maynard, J.B., 2004. Trace-element behavior and redox facies in core shales of Upper Pennsylvanian Kansas-type cyclothems. *Chemical Geology* 206, 289–318.

Aller, R.C., 1998. Mobile deltaic and continental shelf muds as suboxic, fluidized bed reactors. *Marine Chemistry* 61, 143–155.

Aller, R.C., Hannides, A., Heilbrun, C., Panzeca, C., 2004. Coupling of early diagenetic processes and sedimentary dynamics in tropical shelf environments: the Gulf of Papua deltaic complex. *Continental Shelf Research* 24, 2455–2486.

Alt-Epping, U., Stuut, J.-B.W., Hebelin, D., Schneider, R., 2009. Variations in sediment provenance during the past 3000 years off the Tagus River, Portugal. *Marine Geology* 261, 82–91.

Arthur, M.A., Sageman, B.B., 1994. Marine black shales: depositional mechanisms and environments of ancient deposits. *Annual Review of Earth and Planetary Sciences* 22, 499–551.

Arthur, M.A., Sageman, B.B., 2005. Sea level control on source rock development: perspectives from the Holocene Black Sea, the Mid-Cretaceous western interior Basin of North America, and the Late Devonian Appalachian Basin. *The Deposition of Organic Carbon-Rich Sediments: Models, Mechanisms and Consequences: SEPM Special Publication*, 82, pp. 35–59.

Aubry, M.-P., Ouda, K., Dupuis, C., Berggren, W.A., Van Couvering, J.A., 2007. The global standard stratotype section and point (GSSP) for the base of the Eocene series in the Dababiya section (Egypt). *Episodes* 30, 271–286.

Bains, S., Corfield, R.M., Norris, R.D., 1999. Mechanisms of climate warming at the end of the Paleocene. *Science* 285, 724–727.

Blanc-Valleron, M.-M., Thiry, M., 1997. Clay minerals, paleoweathering, paleolandscapes and climatic sequences: the paleogene continental deposits in France. In: Paquet, H., Clauer, N. (Eds.), *Soils and sediments: Mineralogy and geochemistry*. Springer, Heidelberg, Germany, pp. 223–247.

Bolle, M.-P., Adatte, T., 2001. Paleocene–early Eocene climatic evolution in the Tethyan realm: clay mineral evidence. *Clay Minerals* 36, 249–261.

Bolle, M.-P., Pardo, A., Hinrichs, K.-U., Adatte, T., von Salis, K., Burns, S.J., Keller, G., Muzylev, N., 2000a. The Paleocene–Eocene transition in the marginal northeastern Tethys (Kazakhstan and Uzbekistan). *International Journal of Earth Sciences* 89, 390–414.

Bolle, M.-P., Tantawy, A.-A., Pardo, A., Adatte, T., Burns, S.J., Kassab, A.S., 2000b. Climatic and environmental changes documented in the upper Paleocene to lower Eocene of Egypt. *Eclogae Geologicae Helveticae* 93, 33–51.

Smectites. In: Borchardt, G.A. (Ed.), *Minerals in Soil Environments*. Soil Science Society America, Madison, WI, p. 293.

Bornemann, A., Schulte, P., Sprong, J., Steurbaut, E., Youssef, M., Speijer, R.P., 2009. Latest Danian carbon isotope anomaly and associated environmental change in the southern Tethys (Nile Basin, Egypt). *Journal of the Geological Society, London* 166, 1135–1142.

Bowen, G.J., Bowen, B.B., 2008. Mechanisms of PETM global change constrained by a new record from central Utah. *Geology* 36, 379–382.

Bowen, G.J., Beerling, D.J., Koch, P.L., Zachos, J.C., Quattlebaum, T., 2004. A humid climate state during the Palaeocene/Eocene thermal maximum. *Nature* 432, 495–499.

Bowen, G.J., Bralower, T.J., Delaney, M.L., Dickens, G.R., Kelly, D.C., Koch, P.L., Kump, L.R., Meng, J., Sloan, L.C., Thomas, E., Wing, S.L., Zachos, J.C., 2006. Eocene hyperthermal event offers insight into greenhouse warming. *EOS* 87, 165–169.

Brookins, D.G., 1989. Geochemistry and mineralogy of rare earth elements. In: Lipin, B.R., McKay, G.A. (Eds.), *Reviews in Mineralogy*, 21. Mineralogical Society of America, pp. 201–225.

Bruland, K.W., Rue, E.L., Smith, G.J., 2001. Iron and macronutrients in California coastal upwelling regimes: implications for diatom blooms. *Limnology and Oceanography* 46, 1661–1674.

Bruland, K.W., Rue, E.L., Smith, G.J., DiTullio, G.R., 2005. Iron, macronutrients and diatom blooms in the Peru upwelling regime: brown and blue waters of Peru. *Marine Chemistry* 93, 81–103.

Brumsack, H.-J., 2006. The trace metal content of recent organic carbon-rich sediments: implications for Cretaceous black shale formation. *Palaeogeography, Palaeoclimatology, Palaeoecology* 232, 344–361.

Calvert, S.E., Pedersen, T.F., 1993. Geochemistry of recent oxic and anoxic marine sediments: implications for the geological record. *Marine Geology* 113, 67–88.

Canfield, D.E., 1994. Factors influencing organic carbon preservation in marine sediments. *Chemical Geology* 114, 315–329.

Canfield, D.E., Lyons, T.W., Raiswell, R., 1996. A model for iron deposition to euxinic Black Sea sediments. *American Journal of Science* 296, 818–834.

Cattaneo, A., Steel, R.J., 2003. Transgressive deposits: a review of their variability. *Earth-Science Reviews* 62, 187–228.

Chamley, H., 1997. Clay mineral sedimentation in the ocean. In: Paquet, H., Clauer, N. (Eds.), *Soils and sediments*. Springer, Heidelberg, Germany, pp. 269–302.

Charisi, S.D., Schmitz, B., 1995. Stable ( $\delta^{13}C$ ,  $\delta^{18}O$ ) and strontium ( $^{87}Sr/^{86}Sr$ ) isotopes through the Paleocene at Gebel Aweina, eastern Tethyan region. *Palaeogeography, Palaeoclimatology, Palaeoecology* 116, 103–129.

Cox, R., Lowe, D.R., Cullers, R.L., 1995. The influence of sediment recycling and basement composition on evolution of mudrock chemistry in the southwestern United States. *Geochimica et Cosmochimica Acta* 59, 2919–2940.

Cramer, B.S., Aubry, M.-P., Miller, K.G., Olsson, R.K., Wright, J.D., Kent, D.V., 1999. An exceptional chronologic, isotopic and clay mineralogical record of the latest Paleocene thermal maximum, Bass River, NJ, ODP 174 AX. *Bulletin de la Société Géologique de France* 170, 883–897.

Crouch, E.M., Dickens, G.R., Brinkhuis, H., Aubry, M.-P., Hollis, C.J., Rogers, K.M., Visscher, H., 2003. The *Apectodinium* acme and terrestrial discharge during the Paleocene–Eocene thermal maximum: new palynological, geochemical and calcareous nannoplankton observations at Tawanui, New Zealand. *Palaeogeography, Palaeoclimatology, Palaeoecology* 194, 387–403.

Curtis, C.D., 1990. Aspects of climatic influence on the clay mineralogy and geochemistry of soils, palaeosols and clastic sedimentary rocks. *Journal of the Geological Society, London* 147, 351–357.

Dean, W.E., Arthur, M.A., 1998. Geochemical expressions of cyclicity in Cretaceous pelagic limestone sequences: Niobrara Formation, Western Interior Seaway.

- Stratigraphy and Paleoenvironments of the Cretaceous Western Interior Seaway, USA: SEPM, Concepts in Sedimentology and Paleontology, 6, pp. 227–255. SEPM.
- Demaison, G.J., Moore, G.T., 1980. Anoxic environments and oil source bed genesis. *Organic Geochemistry* 2, 9–31.
- Dickens, G.R., O'Neil, J.R., Rea, D.K., Owen, R.M., 1995. Dissociation of oceanic methane hydrate as a cause of the carbon isotope excursion at the end of the Paleocene. *Paleoceanography* 10, 965–971.
- Dupuis, C., Aubry, M.-P., Steurbaut, E., Berggren, W.A., Ouda, K., Magioncalda, R., Cramer, B.S., Kent, D.V., Speijer, R.P., Heilmann-Clausen, C., 2003. The Dababiya Quarry section: lithostratigraphy, clay mineralogy, geochemistry and paleontology. *Micropaleontology* 49, 41–59.
- Dypvik, H., Harris, N.B., 2001. Geochemical facies analysis of fine-grained siliciclastics using Th/U, Zr/Rb and (Zr + Rb)/Sr ratios. *Chemical Geology* 181, 131–146.
- Egger, H., Heilmann-Clausen, C., Schmitz, B., 2009. From shelf to abyss: record of the Paleocene/Eocene-boundary in the Eastern Alps (Austria). *Geologica Acta* 7, 215–227.
- Ernst, S.R., Guasti, E., Dupuis, C., Speijer, R.P., 2006. Environmental perturbation in the southern Tethys across the Paleocene/Eocene boundary (Dababiya, Egypt): foraminiferal and clay mineral records. *Marine Micropaleontology* 60, 89–111.
- Farley, K.A., Eltgroth, S.F., 2003. An alternative age model for the Paleocene–Eocene thermal maximum using extraterrestrial <sup>3</sup>He. *Earth and Planetary Science Letters* 208, 135–148.
- Fischer, C., Schmidt, C., Bauer, A., Gaupp, R., Heide, K., 2009. Mineralogical and geochemical alteration of low-grade metamorphic black slates due to oxidative weathering. *Chemie der Erde – Geochemistry* 69, 127–142.
- Föllmi, K.B., 1996. The phosphorus cycle, phosphogenesis and marine phosphate-rich deposits. *Earth-Science Reviews* 40, 55–124.
- Fralick, P.W., Kronberg, B.L., 1997. Geochemical discrimination of clastic sedimentary rock sources. *Sedimentary Geology* 113, 111–124.
- Galloway, J.N., Cowling, E.B., 2002. Reactive nitrogen and the world: two hundred years of change. *Ambio* 31, 64–71.
- Gavrilov, Y.O., Shcherbinina, E.A., Oberhänsli, H., 2003. Paleocene–Eocene boundary events in the northeastern Peri-Tethys. *Geological Society of America, Special Paper* 369, 147–168.
- Gheerbrant, E., Rage, J.-C., 2006. Paleobiogeography of Africa: how distinct from Gondwana and Laurasia? *Palaeogeography, Palaeoclimatology, Palaeoecology* 241, 224–246.
- Gibson, T.G., Bybell, L.M., Owens, J.P., 1993. Latest Paleocene lithologic and biotic events in neritic deposits of southwestern New Jersey. *Paleoceanography* 8, 495–514.
- Gibson, T.G., Bybell, L.M., Mason, D.B., 2000. Stratigraphic and climatic implications of clay mineral changes around the Paleocene/Eocene boundary of the northeastern US margin. *Sedimentary Geology* 134, 65–92.
- Glenn, C.R., Arthur, M.A., 1990. Anatomy and origin of a Cretaceous phosphorite-greensand giant, Egypt. *Sedimentology* 37, 123–154.
- Glenn, C.R., Föllmi, K.B., Riggs, S.R., Baturin, G.N., Grimm, K.A., Trappe, J., Abed, A.M., Galli-Olivier, C., Garrison, R.E., Ilyin, A.V., Jehl, C., Rohrlach, V., Sadaqah, R.M.Y., Schidlowski, M., Sheldon, R.E., Siegmund, H., 1994. Phosphorus and phosphorites: sedimentology and environments of formation. *Eclogae Geologicae Helveticae* 87, 747–788.
- Gromet, L.P., Haskin, L.A., Korotev, R.L., Dymek, R.F., 1984. The “North American shale composite”: its compilation, major and trace element characteristics. *Geochimica et Cosmochimica Acta* 48, 2469–2482.
- Guasti, E., Speijer, R.P., 2007. The Paleocene–Eocene thermal maximum in Egypt and Jordan: an overview of the planktic foraminiferal record. *Geological Society of America, Special Paper* 424, 53–67.
- Hatch, J.R., Leventhal, J.S., 1992. Relationship between inferred redox potential of the depositional environment and geochemistry of the Upper Pennsylvanian (Missourian) Stark Shale Member of the Dennis Limestone, Wabaunsee County, Kansas, U.S.A. *Chemical Geology* 99, 65–82.
- Higgins, J.A., Schrag, D.P., 2006. Beyond methane: towards a theory for the Paleocene–Eocene thermal maximum. *Earth and Planetary Science Letters* 245, 523–537.
- Höntzsch, S., Scheibner, C., Kuss, J., Marzouk, A.M., Rasser, M.W., 2011. Tectonically driven carbonate ramp evolution at the southern Tethyan shelf: the Lower Eocene succession of the Galala Mountains, Egypt. *Facies* 57, 51–72.
- Jeanes, C.V., Wray, D.S., Merriman, R.J., Fisher, M.J., 2000. Volcanogenic clays in Jurassic and Cretaceous strata of England and the North Sea Basin. *Clay Minerals* 35, 25–55.
- Jenkyns, H.C., 2010. Geochemistry of oceanic anoxic events. *Geochemistry Geophysics Geosystems* 11, Q03004.
- John, C.M., Bohaty, S.M., Zachos, J.C., Sluijs, A., Gibbs, S., Brinkhuis, H., Bralower, T.J., 2008. North American continental margin records of the Paleocene–Eocene thermal maximum: implications for global carbon and hydrological cycling. *Paleoceanography* 23, PA2217.
- Jones, B., Manning, D.A.C., 1994. Comparison of geochemical indices used for the interpretation of paleoredox conditions in ancient mudstones. *Chemical Geology* 111, 111–129.
- Kelly, D.C., Zachos, J.C., Bralower, T.J., Schellenberg, S.A., 2005. Enhanced terrestrial weathering/runoff and surface ocean carbonate production during the recovery stages of the Paleocene–Eocene thermal maximum. *Paleoceanography* 20, PA4023.
- Kennett, J.P., Stott, L.D., 1991. Abrupt deep-sea warming, palaeoceanographic changes and benthic extinctions at the end of the Paleocene. *Nature* 353, 225–229.
- Kent, D.V., Dupuis, C., 2003. Paleomagnetic study of the Paleocene–Eocene Tarawan Chalk and Esna Shale: dual polarity remagnetizations of Cenozoic sediments in the Nile Valley (Egypt). *Micropaleontology* 49, 139–146.
- Knox, R.W.O.B., Aubry, M.-P., Berggren, W.A., Dupuis, C., Ouda, K., Magioncalda, R., Soliman, M., 2003. The Qreiya section at Gebel Abu Had: lithostratigraphy, clay mineralogy, geochemistry and biostratigraphy. *Micropaleontology* 49, 93–104.
- Kopp, R.E., Schumann, D., Raub, T.D., Powars, D.S., Godfrey, L.V., Swanson-Hysell, N.L., Maloof, A.C., Vali, H., 2009. An Appalachian Amazon? Magnetofossil evidence for the development of a tropical river-like system in the mid-Atlantic United States during the Paleocene–Eocene thermal maximum. *Paleoceanography* 24, PA4211.
- Krajewski, K.P., Van Capellen, P., Trichet, J., Kuhn, O., Lucas, J., Martín-Algarra, A., Prévôt, L., Tewari, V.C., Gaspar, L., Knight, R.I., Lamboy, M., 1994. Biological processes and apatite formation in sedimentary environments. *Eclogae Geologicae Helveticae* 87, 701–745.
- Lipinski, M., Warning, B., Brumsack, H.-J., 2003. Trace metal signatures of Jurassic/Cretaceous black shales from the Norwegian Shelf and the Barents Sea. *Palaeogeography, Palaeoclimatology, Palaeoecology* 190, 459–475.
- Littke, R., Klussmann, U., Krooss, B., Leythaeuser, D., 1991. Quantification of loss of calcite, pyrite, and organic matter due to weathering of Toarcian black shales and effects on kerogen and bitumen characteristics. *Geochimica et Cosmochimica Acta* 55, 3369–3378.
- Lyons, T.W., Severmann, S., 2006. A critical look at iron paleoredox proxies: new insights from modern euxinic marine basins. *Geochimica et Cosmochimica Acta* 70, 5698–5722.
- Magioncalda, R., Dupuis, C., Smith, T., Steurbaut, E., Gingerich, P.D., 2004. Paleocene–Eocene carbon isotope excursion in organic carbon and pedogenic carbonate: direct comparison in a continental stratigraphic section. *Geology* 32, 553–556.
- McLennan, S.M., 2001. Relationships between the trace element composition of sedimentary rocks and upper continental crust. *Geochemistry, Geophysics, Geosystems* 2, 2000GC000109.
- Meshref, W.M., 1990. Tectonic framework. In: Said, R. (Ed.), *Tectonic Framework. The geology of Egypt*. Balkema, Rotterdam, The Netherlands, pp. 113–156.
- Meyers, S.R., Sageman, B.B., Lyons, T.W., 2005. Organic carbon burial rate and the molybdenum proxy: theoretical framework and application to Cenomanian–Turonian oceanic anoxic event 2. *Paleoceanography* 20, PA2002.
- Miller, K.G., Wright, J.D., Browning, J.V., 2005. Visions of ice sheets in a greenhouse world. *Marine Geology* 217, 215–231.
- Morse, J.W., Wang, Q., 1997. Pyrite formation under conditions approximating those in anoxic sediments: II. Influence of precursor iron minerals and organic matter. *Marine Chemistry* 57, 187–193.
- Murphy, A.E., Sageman, B.B., Hollander, D.J., Lyons, T.W., Brett, C.E., 2000. Black shale deposition and faunal overturn in the Devonian Appalachian Basin: clastic starvation, seasonal water-column mixing, and efficient biolimiting nutrient recycling. *Paleoceanography* 15, 280–291.
- Nicolo, M.J., Dickens, G.R., Hollis, C.J., 2010. South Pacific intermediate water oxygen depletion at the onset of the Paleocene–Eocene Thermal Maximum as depicted in New Zealand margin sections. *Paleoceanography* 25, PA4210.
- Niu, B., Ishida, H., 2000. Different rates of smectite illitization in mudstones and sandstones from the Niigata Basin, Japan. *Clay Minerals* 35, 163–173.
- Ouda, K., 2003. The Paleocene/Eocene boundary in Egypt: an overview. *Micropaleontology* 49, 15–40.
- Pagani, M., Caldeira, K., Archer, D., Zachos, J.C., 2006a. An ancient carbon mystery. *Science* 314, 1556–1557.
- Pagani, M., Pedentchouk, N., Huber, M., Sluijs, A., Schouten, S., Brinkhuis, H., Sinninghe, D., Jaap, S., Dickens, G.R., Expedition, S., 2006b. Arctic hydrology during global warming at the Palaeocene/Eocene thermal maximum. *Nature* 442, 671–675.
- Paillard, D., 2001. Glacial cycles: toward a new paradigm. *Reviews of Geophysics* 39, 325–346.
- Pedersen, T.F., Calvert, S.E., 1990. Anoxia vs productivity: what controls the formation of organic-carbon-rich sediments and sedimentary rocks? *AAPG Bulletin* 74, 454–466.
- Petschick, R., Kuhn, G., Gingele, F.X., 1996. Clay mineral distribution in surface sediments of the South Atlantic: sources, transport, and relation to oceanography. *Marine Geology* 130, 203–229.
- Rabalais, N.N., Turner, R.E., Diaz, R.J., Justic, D., 2009. Global change and eutrophication of coastal waters. *ICES Journal of Marine Science* 66, 1528–1537.
- Rachold, V., Brumsack, H.-J., 2001. Inorganic geochemistry of Albian sediments from the Lower Saxony Basin NW Germany: palaeoenvironmental constraints and orbital cycles. *Palaeogeography, Palaeoclimatology, Palaeoecology* 174, 121–143.
- Rea, D.K., 1994. The paleoclimatic record provided by eolian deposition in the deep sea: the geologic history of wind. *Reviews of Geophysics* 32, 159–195.
- Rimmer, S.M., 2004. Geochemical paleoredox indicators in Devonian–Mississippian black shales, Central Appalachian Basin (USA). *Chemical Geology* 206, 373–391.
- Röhl, U., Bralower, T.J., Norris, R.D., Wefer, G., 2000. New chronology for the late Paleocene thermal maximum and its environmental implications. *Geology* 28, 927–930.
- Röhl, U., Westerhold, T., Bralower, T.J., Zachos, J.C., 2007. On the duration of the Paleocene–Eocene thermal maximum (PETM). *Geochemistry, Geophysics, Geosystems* G3 (8), Q12002.
- Salem, R., 1976. Evolution of Eocene–Miocene sedimentation patterns in parts of Northern Egypt. *AAPG Bulletin* 60, 34–64.
- Scheibner, C., Marzouk, A.M., Kuss, J., 2001. Shelf architectures of an isolated Late Cretaceous carbonate platform margin, Galala Mountains (Eastern Desert, Egypt). *Sedimentary Geology* 145, 23–43.
- Scheibner, C., Speijer, R.P., Marzouk, A.M., 2005. Turnover of larger foraminifera during the Paleocene–Eocene thermal maximum and paleoclimatic control on the evolution of platform ecosystems. *Geology* 33, 493–496.
- Schmitz, B., Andreasson, F.P., 2001. Air humidity and lake d18O during the latest Paleocene–earliest Eocene in France from recent and fossil fresh-water and marine gastropod  $\delta^{18}\text{O}$ ,  $\delta^{13}\text{C}$ , and  $^{87}\text{Sr}/^{86}\text{Sr}$ . *Bulletin of the Geological Society of America* 113, 774–789.
- Schmitz, B., Pujalte, V., 2007. Abrupt increase in seasonal extreme precipitation at the Paleocene–Eocene boundary. *Geology* 35, 215–218.

- Schmitz, B., Pujalte, V., Núñez-Betelu, K., 2001. Climate and sea-level perturbations during the Incipient Eocene thermal maximum: evidence from siliciclastic units in the Basque Basin (Ermua, Zumaia and Trabakua Pass), northern Spain. *Palaeogeography, Palaeoclimatology, Palaeoecology* 165, 299–320.
- Setti, M., Marinoni, L., López-Galindo, A., 2004. Mineralogical and geochemical characteristics (major, minor, trace elements and REE) of detrital and authigenic clay minerals in a Cenozoic sequence from Ross Sea, Antarctica. *Clay Minerals* 39, 405–421.
- Sluijs, A., Schouten, S., Pagani, M., Woltering, M., Brinkhuis, H., Sinninghe, D.J.S., Dickens, G.R., Huber, M., Reichart, G.-J., Stein, R., Matthiessen, J., Lourens, L.J., Pedentchouk, N., Backman, J., Moran, K., 2006. Subtropical Arctic Ocean temperatures during the Palaeocene/Eocene thermal maximum. *Nature* 441, 610–613.
- Sluijs, A., Bowen, G.J., Brinkhuis, H., Lourens, L.J., Thomas, E., 2007. The Palaeocene–Eocene thermal maximum super greenhouse: Biotic and geochemical signatures, age models and mechanisms of climate change. In: Williams, M., Haywood, A.M., Gregory, J., Schmidt, D.N. (Eds.), *Deep Time Perspectives on Climate Change: Marrying the Signal from Computer Models and Biological Proxies*. TMS Special Publications, London, 2, pp. 323–349.
- Sluijs, A., Brinkhuis, H., Crouch, E.M., John, C.M., Handley, L., Munsterman, D., Bohaty, S.M., Zachos, J.C., Reichart, G.-J., Schouten, S., Pancost, R.D., Damste, J.S.S., Welters, N.L.D., Lotter, A.F., Dickens, G.R., 2008. Eustatic variations during the Paleocene–Eocene greenhouse world. *Paleoclimatology* 23, PA4216.
- Smith, R.L., 1992. Coastal upwelling in the modern ocean. *Geological Society of London, Special Publication* 64, 9–28.
- Soliman, M.F., Ahmed, E., Kurzweil, H., 2006. Geochemistry and mineralogy of the Paleocene/Eocene boundary at Gabal Dababiya (GSSP) and Gabal Owaina sections, Nile Valley, Egypt. *Stratigraphy* 3, 31–52.
- Soudry, D., Glenn, C.R., Nathan, Y., Segal, I., Vonderhaar, D., 2006. Evolution of Tethyan phosphogenesis along the northern edges of the Arabian–African shield during the Cretaceous–Eocene as deduced from temporal variations of Ca and Nd isotopes and rates of P accumulation. *Earth-Science Reviews* 78, 27–57.
- Speijer, R.P., 2003. Danian–Selandian sea-level change and biotic excursion on the southern Tethyan margin (Egypt). In: Wing, S.L., Gingerich, P.D., Schmitz, B., Thomas, E. (Eds.), *Causes and consequences of globally warm climates in the early Paleogene*. *Geol. Soc. Am. Spec. Pap.*, 369, pp. 275–290.
- Speijer, R.P., Morsi, A.-M.M., 2002. Ostracode turnover and sea-level changes associated with the Paleocene–Eocene thermal maximum. *Geology* 30, 23–26.
- Speijer, R.P., Wagner, T., 2002. Sea-level changes and black shales associated with the late Paleocene thermal maximum: organic-geochemical and micropaleontologic evidence from the southern Tethyan margin (Egypt–Israel). In: Koeberl, C., MacLeod, K.G. (Eds.), *Catastrophic events and mass extinctions: impacts and beyond*. *Geol. Soc. Am. Spec. Pap.*, 356, pp. 533–549.
- Srodon, J., 1999. Nature of mixed-layer clays and mechanisms of their formation and alteration. *Annual Review of Earth and Planetary Sciences* 27, 19–53.
- Storey, M., Duncan, R.A., Swisher III, Carl C., 2007. Paleocene–Eocene thermal maximum and the opening of the northeast Atlantic. *Science* 316, 587–589.
- Summerhayes, C.P., Kroon, D., Rosell-Melé, A., Jordan, R.W., Schrader, H.-J., Hearn, R., Villanueva, J., Grimalt, J.O., Eglinton, G., 1995. Variability in the Benguela current upwelling system over the past 70,000 years. *Progress in Oceanography* 35, 207–251.
- Tantawy, A.A., Keller, G., Adatte, T., Stinnesbeck, W., Kassab, A., Schulte, P., 2001. Maastrichtian to Paleocene depositional environment of the Dakhla Formation, Western Desert, Egypt: sedimentology, mineralogy, and integrated micro- and macrofossil biostratigraphies. *Cretaceous Research* 22, 795–827.
- Thiry, M., 2000. Palaeoclimate interpretation of clay minerals in marine deposits: an outlook from the continental origin. *Earth-Science Reviews* 49, 201–221.
- Thomson, J., Jarvis, I., Green, D.R.H., Green, D.A., Clayton, T., 1998. Mobility and immobility of redox-sensitive elements in deep-sea turbidites during shallow burial. *Geochimica et Cosmochimica Acta* 62, 643–656.
- Trenberth, K.E., Jones, P.D., Ambenje, P., Bojariu, R., Easterling, D., Klein Tank, A., Parker, D., Rahimzadeh, F., Renwick, J.A., Rusticucci, M., Soden, B., Zhai, P., 2007. Observations: surface and atmospheric climate change. In: Solomon, S., Qin, D., Manning, M., Chen, Z., Marquis, M., Averyt, K.B., Tignor, M., Miller, H.L. (Eds.), *Contribution of working group I to the fourth assessment report of the intergovernmental panel on climate change: Climate Change 2007: The Physical Science Basis*, Contribution of Working Group I to the fourth Assessment Report of the Intergovernmental Panel on Climate Change, pp. 1–102.
- Tribouillard, N., Trentesaux, A., Ramdani, A., Baudinet, F., Riboulleau, A., 2004. Controls on organic accumulation in late Jurassic shales of northwestern Europe as inferred from trace-metal geochemistry. *Bulletin de la Societe Geologique de France* 175, 491–506.
- Tribouillard, N., Algeo, T.J., Lyons, T., Riboulleau, A., 2006. Trace metals as paleoredox and paleoproductivity proxies: an update. *Chemical Geology* 232, 12–32.
- Tyson, R.V., Pearson, T.H., 1991. Modern and ancient continental shelf anoxia: an overview. In: Tyson, R.V., Pearson, T.H. (Eds.), *Modern and ancient continental shelf anoxia*. *Geol. Soc. London Spec. Publ.*, 58, pp. 1–24.
- Utzmann, A., Hansteen, T.H., Schmincke, H.-U., 2002. Trace element mobility during sub-seafloor alteration of basaltic glass from Ocean Drilling Program site 953 (off Gran Canaria). *International Journal of Earth Sciences* 91 (4), 661–679.
- Uysal, I.T., Golding, S.D., 2003. Rare earth element fractionation in authigenic illite-smectite from Late Permian clastic rocks, Bowen Basin, Australia: implications for physico-chemical environments of fluids during illitization. *Chemical Geology* 193, 167–179.
- Van Cappellen, P., Ingall, E.D., 1994. Benthic phosphorus regeneration, net primary production, and ocean anoxia: a model of the coupled marine biogeochemical cycles of carbon and phosphorus. *Paleoceanography* 9, 677–692.
- Van Cappellen, P., Ingall, E.D., 1996. Redox stabilization of the atmosphere and oceans by phosphorus-limited marine productivity. *Science* 271, 493–496.
- Wadman, H.M., McNinch, J.E., 2008. Stratigraphic spatial variation on the inner shelf of a high-yield river, Waipatu River, New Zealand: implications for fine-sediment dispersal and preservation. *Continental Shelf Research* 28, 865–886.
- Wehausen, R., Brumsack, H.-J., 1999. Cyclic variations in the chemical composition of eastern Mediterranean Pliocene sediments: a key for understanding sapropel formation. *Marine Geology* 153, 161–176.
- Werne, J.P., Sageman, B.B., Lyons, T.W., Hollander, D.J., 2002. An integrated assessment of a “type euxinic” deposit: evidence for multiple controls on black shale deposition in the middle Devonian Oatka Creek formation. *American Journal of Science* 302, 110–143.
- White, T., Arthur, M.A., 2006. Organic carbon production and preservation in response to sea-level changes in the Turonian Carlisle Formation, US Western Interior Basin. *Palaeogeography, Palaeoclimatology, Palaeoecology* 235, 223–244.
- Wignall, P.B., Newton, R., 2001. Black shales on the basin margin: a model based on examples from the Upper Jurassic of the Boulonnais, northern France. *Sedimentary Geology* 144, 335–356.
- Zachos, J.C., Röhl, U., Schellenberg, S.A., Sluijs, A., Hodell, D.A., Kelly, D.C., Thomas, E., Nicolo, M., Raffi, I., Lourens, L.J., McCarran, H., Kroon, D., 2005. Rapid acidification of the ocean during the Paleocene–Eocene thermal maximum. *Science* 308, 1611–1615.
- Zecchin, M., 2007. The architectural variability of small-scale cycles in shelf and ramp clastic systems: the controlling factors. *Earth-Science Reviews* 84, 21–55.
- Zimmermann, U., Bahlburg, H., 2003. Provenance analysis and tectonic setting of the Ordovician clastic deposits in the southern Puna Basin, NW Argentina. *Sedimentology* 50, 1079–1104.
- Zwingmann, H., Clauer, N., Gaupp, R., 1999. Structure-related geochemical (REE) and isotopic (K–Ar, Rb–Sr, d18O) characteristics of clay minerals from Rotliegend sandstone reservoirs (Permian, northern Germany). *Geochimica et Cosmochimica Acta* 63, 2805–2823.